www.itcon.org - Journal of Information Technology in Construction - ISSN 1874-4753

AUTOMATED GEOMETRY-BASED ANALYSIS FOR OBJECT-LEVEL SCAN-VS-BIM VALIDATION OF TBE COMPONENTS

SUBMITTED: July 2025
PUBLISHED: February 2026
EDITOR: Frédéric Bosché
DOI: 10.36680/j.itcon.2026.004

Tristan Kinnen (corresponding author)
Geodetic Institute and Chair for Computing in Civil Engineering & Geo Information Systems, RWTH Aachen University, Germany
https://orcid.org/0000-0002-1837-2131
kinnen@gia.rwth-aachen.de

Jörg Blankenbach
Geodetic Institute and Chair for Computing in Civil Engineering & Geo Information Systems, RWTH Aachen University, Germany
https://orcid.org/0000-0002-5700-8818
blankenbach@gia.rwth-aachen.de

SUMMARY: *Technical building equipment (TBE) systems offer significant potential for energy savings that can be realized through digital twins and simulations. Digital twins require a precise virtual representation of the real object. Geometric-semantic models originating from Building Information Modeling (BIM)-based planning can be a valuable basis for this. However, due to unavoidable deviations between planning and construction, a high-quality comparison of as-planned and as-built data is crucial. This study presents a geometric and statistical analysis framework for component-specific validation of TBE systems using as-planned BIM models and as-built point clouds. The framework was evaluated on datasets of increasing complexity, from simulations to real-world projects. Results show that with sufficient data quality, the framework enables the validation of up to 88% of components, significantly reducing manual effort, cost, and time. However, as a geometry-based approach, its performance is affected by data quality issues such as point cloud noise and occlusions.*

KEYWORDS: *as-planned vs. as-built, building information modeling, scan-vs-BIM, technical building equipment.*

REFERENCE: *Kinnen, T., & Blankenbach, J. (2026). Automated geometry-based analysis for object-level Scan-vs-BIM validation of TBE components. Journal of Information Technology in Construction (ITcon), 31, 75-105. https://doi.org/10.36680/j.itcon.2026.004*

COPYRIGHT: *© 2026 The author(s). This is an open access article distributed under the terms of the Creative Commons Attribution 4.0 International (https://creativecommons.org/licenses/by/4.0/), which permits unrestricted use, distribution, and reproduction in any medium, provided the original work is properly cited.*

1. INTRODUCTION

The construction industry has struggled to keep up with other sectors regarding the adoption of digital technologies. Despite this delay, the transformative potential of digital approaches is increasingly being recognized. Key technological developments include Building Information Modeling (BIM) and Digital Twins (DTw), which have proven to be key components in the digitization of the construction industry. BIM provides a structured methodology for the design, construction, and management of buildings using integrated digital models, and promotes collaboration and efficiency among stakeholders. DTw, on the other hand, extend this idea by providing dynamic, real-time representations of buildings that enable advanced monitoring and optimization capabilities (Tao & Qi, 2019). In addition, DTw integrate various data sources and models and establish a close connection between the physical and virtual representations. Particularly with regard to energy efficiency and sustainability, the linking of digital working methods and energy system optimizations resulting in the creation of a DTw of the technical building equipment (TBE) offers great potential by enabling simulations and the identification of optimization opportunities (Becker et al., 2022; Blut et al., 2024). TBE encompasses all technical systems that enable the operation of a building. Among other systems, this includes heating, ventilation, and water systems. As all of these systems are interconnected, a change or failure in one subsystem can have an impact on the other systems. The resulting complexity emphasizes the need for systematic evaluation and inspection methods to ensure the reliable operation of the entire construction.

In the context of developing a DTw, as well as in the broader application of BIM in the lifecycle, accurate and continuous alignment between design data (as-planned) and the data representing the actual implementation (as-built) is essential (Arayici et al., 2012). Comparing planned and actual data not only ensures compliance with design requirements, but also serves as a basis for operational optimization and future modernization efforts. The quality, and thus the usability, of a DTw depends crucially on the accurate representation of the as-built condition. Only if the actual situation is accurately reflected in the digital model can it serve as a reliable basis for advanced applications such as energy optimization, predictive maintenance, or life cycle-oriented modernization. This is particularly relevant in the area of TBE systems, which are characterized by high complexity and sensitivity to deviations. Deviations between the planned and installed states can lead to inefficiencies or costly maintenance work. Furthermore, a comparison between the planning and execution data is necessary to ensure the safety and functionality of the system. Manual verification of actual conditions is very time-consuming and costly. Automated or partly automated approaches therefore offer great potential for detecting deviations more efficiently and saving time and money. For component-specific validation, specialized methods are required that operate within defined tolerance ranges. In pursuit of a holistic application of BIM, as-planned data include semantically enriched 3D models. While geometric information describes shape, size, and spatial positions, semantic data contain information about the type, properties and relationships of the respective objects. Therefore, as-planned BIM models, containing both semantic and geometric information, can be leveraged to develop algorithms for object validation and to enhance the efficiency of data processing. By contrast, as-built datasets are progressively derived from 3D point clouds generated by technologies such as terrestrial (TLS) or mobile laser scanning (MLS), suitable camera-based systems or depth sensors like built in the Microsoft HoloLens device (Kinnen et al., 2023).

However, as modern buildings increasingly encompass complex structures and vast volumes of data, manual approaches to data evaluation quickly reach their limitations. Automated or partly automated methods capable of efficiently processing and analyzing large datasets are therefore gaining increasing importance. Automation, particularly through the application of Artificial Intelligence (AI), plays a pivotal role in analyzing and comparing as-planned and as-built data. AI-based approaches offer the potential to process large datasets efficiently and to classify discrepancies automatically.

From today's perspective, modern AI approaches are predominantly shaped by deep learning methods, which require many and diverse datasets for training. In the field of TBE systems, however, there is a lack of publicly available datasets suitable for such purposes. Consequently, geometry-based analytical models for detecting discrepancies and validating alignment with design data currently represent a more promising approach for TBE systems applications.

In this context, this study introduces a method specifically tailored to the comparison of as-planned and as-built data for TBE systems. The proposed method integrates geometry-based algorithms with rigid statistical evaluations to enable partly automated classification of TBE objects. Due to the often challenging conditions for creating high-

CC BY

quality as-built point clouds in practice for TBE systems, the aim of this work is not to create a comprehensive and fully automated solution for comparing as-planned and as-built data. Instead, a method is presented that categorizes the respective TBE system in an automated and component-based manner, symbolically inspired by a traffic light system. The TBE system is to be divided into areas in which the method determines with a high degree of certainty whether as-planned and as-built data match (green) or differ (red). In the remaining areas, where the method delivers uncertain results (yellow), the task of inspection remains with the expert human operator. For this purpose, each object is automatically categorized to determine whether it has been constructed according to the design, is rotated or displaced, is missing, or has been replaced by a non-conforming component. Consequently, this approach not only provides detailed component validation but also establishes a foundation for the further development of DTw.

This study begins with a review of relevant works and a summary of the current state of research. Subsequently, the various geometry-based analyses in conjunction with the corresponding statistical evaluation methods are described in detail. The results obtained from the application of the proposed method are then analyzed using four different datasets, and the limitations of its application are identified. The final section consolidates and discusses the findings, offering insights and a perspective on potential future research directions.

2. STATE OF ART

The necessary systematic comparison of as-planned and as-built data within the BIM context can involve significant manual effort, depending on the complexity of the construction project. Therefore, exploring automated approaches offers considerable potential for research. A key distinction in this field lies in whether the focus is on a comparative approach between the reality capture data and the as-planned BIM (Scan-vs-BIM), or whether (partially) automated methods for direct as-built modeling based on scan data (Scan-to-BIM) are considered. A detailed literature review on Scan-to-BIM approaches is presented by (Kellner et al., 2024) and (Pătrăucean et al., 2015).

For Scan-vs-BIM approaches, (Pătrăucean et al., 2015) propose that the key to effective methodologies lies in transforming BIM data into a point cloud, allowing for data analysis with matching data types for both as-planned and as-built datasets. In this context, geometric analyses for feature extraction from point cloud data can be applied, as demonstrated by (Gumhold et al., 2001), where a method for geometric comparison was presented that involves the detection of corners and edges through the examination of local point densities and neighborhood relationships. Another approach to Scan-vs-BIM is described by (Chen & Yong, 2019), where a column-detection algorithm, alongside the Random Sample Consensus (RANSAC) method, was used for registering point clouds to a BIM model. This process included the conversion of the BIM model into a point cloud to facilitate direct point-to-point comparisons. Conversely, the geometric deviation analysis by (Anil et al., 2013) involved calculating the minimal Euclidean distance between points in the as-built point cloud and the closest corresponding objects in the as-planned BIM. The resulting distance was then compared to a threshold value, which varied depending on data quality, to identify potential errors in data capture, processing, and model creation. In contrast, Scan-vs-BIM can also be performed by voxel-based (Meyer et al., 2022) or octree-based approaches (Park et al., 2021). Furthermore, (Tran & Khoshelham, 2019) propose an automated approach for detecting changes for walls and floors of indoor building environments by comparing BIM data with point clouds using point classification and surface coverage analysis. Conversely, (Kim et al., 2020) introduced an approach for monitoring project progress by combining 3D point cloud data with the 4D parameters of BIM through the application of the Scan-vs-BIM method. Another Scan-vs-BIM approach is presented by (Tan et al., 2024) for quality inspections of walls, floors, and reinforcing bars in modular construction, in which LiDAR point clouds of the actual condition are compared with as-planned BIM models in order to segment modular units and components.

Other Scan-vs-BIM approaches have been introduced with a focus on industrial facilities. For instance, (Lin et al., 2025) showed an approach, in which the precise object axes are extracted from point clouds and used to update the associated BIM model. In the same context, (Jiang et al., 2022) presented a semi-automated approach to progress monitoring in infrastructure construction, enabling real-time evaluation of 3D point clouds using Hausdorff distance and Poisson surface reconstruction. An object-oriented Scan vs BIM method is introduced by (Chuang and Yang, 2023) comparing local geometries and object similarities. However, none of the presented approaches specifically focus on the application to complex TBE systems with their diverse range of component geometries and validation requirements.

CC BY

Focusing on TBE systems, (Bosché et al., 2014) introduced a Scan-vs-BIM method in which as-built point clouds were processed to assign and segment points based on criteria such as distance and normal vector alignment to the surfaces of TBE components from the as-planned BIM. Points that could not be matched are filtered out, and occluding point clouds are segmented. Subsequently, object recognition is performed by analyzing the surface coverage. Another method was presented by (Nguyen & Choi, 2018), specifically designed for inspecting piping systems in industrial facilities and is based on geometric analysis of object-specific segmented as-built point clouds and corresponding point clouds generated from as-planned BIM data. The evaluation of the geometric agreement between as-planned and as-built data is conducted using metrics such as the mean distance error and the point distance error of individual points. Conversely, (Kawashima et al., 2013; Kawashima et al., 2014) proposed an approach for the segmentation and identification of piping components through the use of a normal-based region-growing technique, followed by cylinder fitting. In contrast, (Kalasapudi et al., 2014) introduced a graph-based framework for automated spatial change analysis of components that links point clouds from 3D laser scans with as-designed BIM models based on their spatial relations.

However, a key issue that consistently limits the performance of automated approaches for comparing as-planned and as-built data is the phenomenon of inaccuracies in point cloud data, as well as occlusions and points in empty space. In the field of TBE in particular, occlusions and multiple reflections often have a significant impact due to the densely packed environment and the presence of metallic surfaces. The previously named studies show various methods for dealing with these disruptive factors. In the approach proposed by (Bosché et al., 2014), points that cannot be assigned to the as-planned model are filtered out, and hidden points between the scanner and model objects are explicitly identified. On this basis, a theoretically visible area of the planned model is calculated. As mentioned before, object recognition is then enabled by evaluating the surface coverage, whereby a confidence value quantifies the reliability of the recognition despite possible occlusions. (Nguyen & Choi, 2018), on the other hand, described their approach as only applicable to object segments that are not affected by occlusion. (Kawashima et al., 2013) and (Kawashima et al., 2014) treated occluded sections of the analyzed pipes by interpolating axis points and performing supplementary fitting. A different way is shown by the approach of (Kalasapudi et al., 2014), which combines local object features with global spatial contexts. This enables object recognition via the spatial relationship to neighboring objects, even if the object is partially occluded.

However, all of these approaches are either designed for general deviation detection or optimized for specific geometric shapes such as pipes and cylindrical elements. Consequently, they do not adequately address the validation of deviations for the wide variety of part geometries found in TBE systems, nor do they support a systematic classification of detected deviations based on component-specific characteristics.

In addition to the previously discussed works in the Scan-vs-BIM context, the exploration of the potential of machine learning approaches, including deep learning, is significantly shaping current research trends. Also, the construction sector is experiencing an increasing examination of such approaches. For instance, (Kim et al., 2024) presented a deep learning approach for the Scan-vs-BIM analysis of steel structures. However, despite the strengths of deep learning in processing large datasets, its practical application in industrial scenarios is often constrained by the limited availability of representative training data and the associated costs required to achieve sufficient model accuracy and generalization. (Abreu et al., 2023) highlighted the issue of insufficient representative datasets in their examination of existing Scan-vs-BIM applications, emphasizing that this gap restricts effective comparisons of as-planned and as-built data in the context of TBE systems. Nevertheless, some machine learning approaches do not require comprehensive training datasets. An example of this in the context of AI-based Scan-vs-BIM for mechanical, electrical, and plumbing (MEP) scenes is presented by (Wang et al., 2025) that uses a few-shot learning method to overcome the issue of missing training data to automatically recognize components. (Hu et al.,2024) also presented an AI-based scan-vs-BIM approach that focuses on the semantic segmentation of MEP components and combines 2D images processed with Faster R-CNN with 3D point clouds from photogrammetry and LiDAR. Focusing on the concept of semantic segmentation, (Hu & Brilakis, 2024) proposed an approach that uses PROSAC shape recognition and DBSCAN clustering to enable automatic instance segmentation in complex construction environments. Another approach was introduced by (Jia et al., 2024), which uses high-dimensional feature tensors to describe local structures in point clouds and applies a rough-to-fine correspondence strategy to perform a Scan-vs-BIM comparison.

Another essential part of this work is the application of statistical evaluation methods. Statistical methods are essential in engineering, especially for reliable data analysis, modeling and decision-making. Commonly used

CC BY

techniques include hypothesis testing, correlation analysis and regression methods. These methods are covered in numerous textbooks and technical literature, such as (Witte et al., 2020) and (Schiefer & Schiefer, 2018), and enable significant relationships in complex engineering datasets to be identified and informed decisions to be made.

In conclusion, numerous approaches have been developed in the domain of automatic Scan-vs-BIM processes, reflecting the extensive and multifaceted interest in this field. In the specific context of TBE systems, existing methodologies predominantly concentrate on defined geometric structures such as pipes and cylindrical elements. Despite the potential of AI-based methods, their application remains constrained due to the scarcity of comprehensive datasets necessary for effective training. Without the feasibility of AI-driven object recognition, the necessity shifts towards leveraging geometric analysis methods. Prior knowledge from existing planning data, such as as-planned BIM models, proves to be a valuable asset in this context. With this foundation, the development of an automated Scan-vs-BIM process tailored for TBE systems holds great potential, since it promises a reduction in manual effort and contributes to the development of DTw, which can serve for continuous monitoring and optimization of energy efficiency within TBE sectors.

However, existing approaches for comparing as-planned and as-built data are mostly based on a single dominant strategy. Each method has its strengths in certain applications. Nevertheless, in particular with complex TBE systems, appropriate methods often encounter limitations. Challenges arise especially due to occlusions, multiple reflections caused by metallic surfaces, and variability in the installation of components. Therefore, many studies focus solely on a specific type of TBE objects, such as pipes. Methods for the holistic analysis of TBE systems, including systematic quantification of deviations at the component level, are rarely presented.

To address this gap, the present work introduces a geometry-based ensemble framework for the holistic analysis of as-planned and as-built data of TBE systems. In contrast to a single dominant strategy, four complementary analysis methods are integrated into the framework. Each method is evaluated using a specific statistical procedure. This design enables robust detection across different component geometries. Furthermore, by jointly considering all probabilistic analyses of the results of these four methods, a robust final classification of the respective component can ultimately be made. Nevertheless, the previously identified limitations remain disruptive factors that cannot be completely ruled out in the proposed approach. In particular, this concerns the strong influence of occlusions and multiple reflections on geometry-based analysis methods, as well as the challenge of robustly distinguishing significantly displaced or rotated components from completely different components. The aim of this study is therefore to evaluate the performance of the novel framework, which combines geometric analysis with statistical evaluation methods, under the influence of these key challenges.

3. METHOD

Our goal in the energyTWIN[1] research project is to develop new methods for the digital, BIM-based commissioning of technical systems in buildings and their energy system optimization. The main focus is on the automated generation of a DTw of technical building systems during commissioning following the execution phase and their continuous enrichment with information during the operating and usage phase. An important basis for this approach is the development of a methodology for the partly automated comparison of as-planned and as-built data. The overall goal of this method is to support workers in inspecting the TBE system by automatically detecting the areas in which automated analysis methods can provide reliable results and those in which manual inspection remains necessary (traffic light system).For this approach, we first created an initial scenario. This scenario requires the existence of an as-planned BIM and involves the initial alignment of the as-planned BIM with the captured as-built point cloud, which represents the actual state of the TBE system after its installation. For our application, BIM models were always exported in the Industry Foundation Classes (IFC) format, which is the standard for data exchange within the BIM environment. Also, the registration of the as-planned BIM and the as-built point cloud serves as a foundation for our analysis, as it forces both data to be in a common coordinate reference system, which allows us to effectively identify discrepancies. After this alignment, we focus on a detailed component-level analysis. Specifically, a component from the as-planned model is selected using its Globally

[1] https://www.energytwin.org

CC BY

Unique Identifier (GUID), which allows for unambiguous identification of the object (buildingSMART Technical, 2024). Subsequently, the bounding boxes of individual TBE components are calculated and transferred from the as-planned BIM to the point cloud. To account for minor geometric deviations between the planned BIM and the actual point cloud, an empirically determined fill of 10% of the bounding box dimensions was applied. This value was chosen to ensure complete segmentation of the correct instance and proportional coverage across components with different dimensions, while keeping the risk of including points from neighboring objects as minimal as possible. By applying the padded bounding box, the corresponding points in the point cloud are segmented, yielding an object-specific point cloud for further analysis. The process of segmenting the point cloud based on individual objects is illustrated in Figure 1.

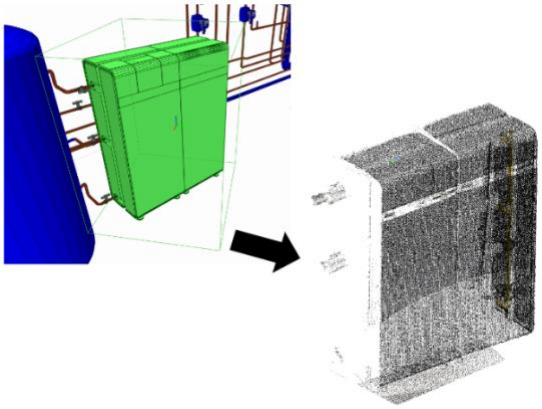


Figure 1: Object-based Point Cloud Segmentation.

The application of this methodology enables the identification of whether each element within a TBE system has been constructed in accordance with the planning data. Specifically, components can be categorized into three distinct groups. The first two groups assess whether a component from the planning model has been installed (1) or not (2). If a component has been installed (1), it is further examined to determine if it is rotated or displaced relative to the planned design. The third category (3) considers the possibility of a component being built, but it is significantly different. This could involve the installation of an entirely different component, such as a pipe in place of a pump, or a component that is functionally equivalent but varies in dimensions, such as a pump from an alternative manufacturer. The outlined approach is presented schematically in Figure 2.

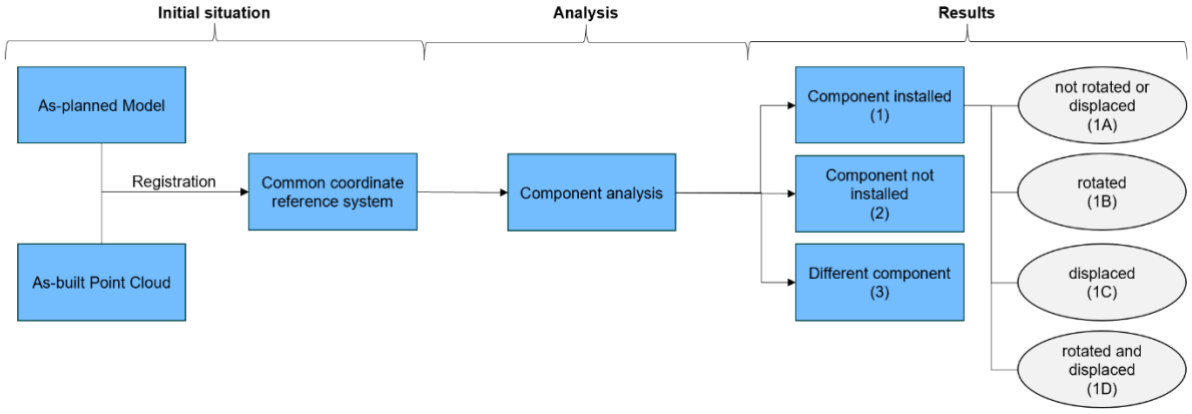


Figure 2: Schematic overview of the methodological analysis (Blut et al., 2024).

For the validation of the individual TBE components, careful consideration of specific spatial or geometric tolerances is essential to ensure the most accurate assessment of construction quality. The tolerance limits are based on two primary factors. First, an appropriate construction tolerance τ_c must be included in the analysis. This construction tolerance reflects possible deviations that can inevitably occur during the execution phase. Typically, this value must be defined specifically for the respective application and scenario and is determined in advance by

CC BY

the client or in accordance with applicable standards and guidelines. On the other hand, the as-built data is based on 3D scan data. Every quantity determined by measurement is subject to measurement deviations that affect the precision and accuracy (ISO, 2023). Precision is defined as the degree of agreement between several measured values obtained under the same conditions. In contrast, accuracy defines the degree of agreement between the measured value and the actual or reference value. The precision and accuracy of scan data depends on the method used for data acquisition, meaning that a specific measurement tolerance τ_m must also be permitted in the analysis. Therefore, based on the predefined tolerance value by the client, it is the responsibility of the surveyor, for example, to select a suitable measuring device to ensure compliance with the specified tolerances. The maximum permissible standard deviation and thus the required precision of the measurement method can be derived from this tolerance. The correlation between the standard deviation and the tolerance is according to (Witte et al., 2020) approximated as

$$\sigma_m = \frac{\tau_m}{5} \tag{1}$$

However, Equation 1 assumes that there are only random (noise) and no systematic (bias) or gross deviations (e.g. outliers) in the data.

Since our theoretical approach cannot incorporate a client's specified tolerance, we adopted a different strategy. Instead of the common practice, we determined the measurement tolerance backwards via the standard deviation respectively the accuracy of the particular measuring instrument. By transforming Equation 1, the relation arises

$$\tau_m = 5\sigma_m \tag{2}$$

However, as unknown systematic deviations may still be present in the measured values, an additional amount Δ_u can be taken into account to cover additional systematic deviations, which represents a benchmark for the correctness of the measurement result (Witte et al., 2020). Those unknown systematic deviations represent consistent measurement biases that shift results. These biases may arise from factors such as remaining instrument calibration errors, unaccounted temperature or other environmental influences, including reflections from metallic surfaces. Data processing procedures, such as model errors, can also contribute to these biases. Therefore, these kinds of deviations differ from random errors since they do not average out over repeated measurements. As a result, the total measurement tolerance to be taken into account is

$$\tau_m = 5\sigma_m + \Delta_u \tag{3}$$

The overall tolerance, as a test criterion for classifying the components, is determined through a combined calculation of the two influencing factors of the construction tolerance and the measurement tolerance. For this calculation, we used the Euclidean L2 norm, as execution and measurement errors are considered independent and random sources of error. The quadratic combination takes into account that statistically independent deviations sum up according to the amount of their variances and not linearly, resulting in a consistent estimate of the overall tolerance. Therefore, and according to the German Standard DIN 18710-1 (German Institute for Standardization [DIN], 2024) and (Witte et al., 2020), the overall tolerance τ_{total} is calculated as

$$\tau_{total} = \sqrt{\tau_c^2 + \tau_m^2} \tag{4}$$

3.1 Geometry-based approaches for as-planned vs. as-built component comparison

This chapter initially presents the analytical methods used for the validation and classification of TBE components, along with their respective automated statistical evaluations. Subsequently, the process chain is outlined, demonstrating how these individual methods can be interconnected to generate a robust, automated assessment. This assessment aims to determine whether the components installed during the execution phase align with the as-planned data or if discrepancies are present, such as rotation, displacement, combined rotation and displacement, absence, or the installation of an alternative component at the anticipated location. Figure 3 indicates which framework approaches can be used for the cases defined in Figure 2. Nevertheless, the targeted classification is limited to the segmented object point cloud. Displaced or rotated and displaced objects can only be correctly identified if the extent of the displacement still ensures sufficient representation of the actual object point cloud within the area segmented by the bounding box.

CC BY

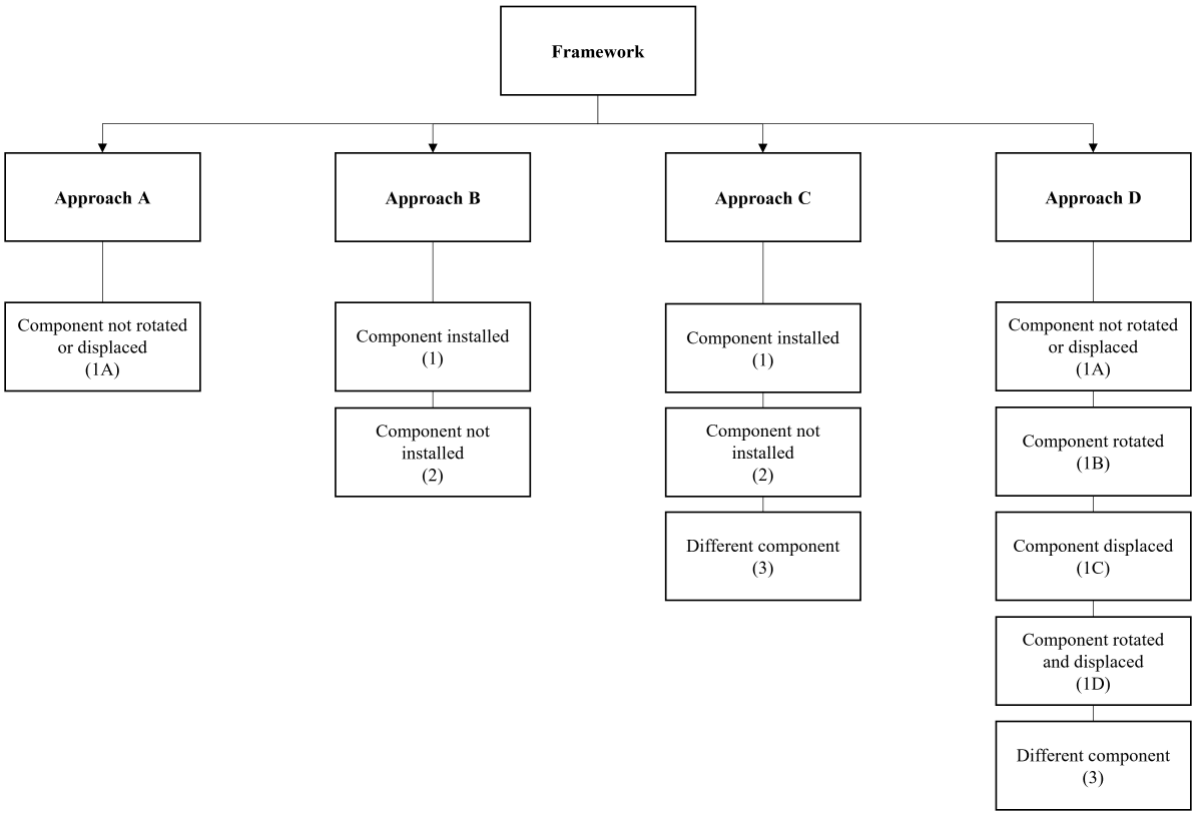


Figure 3: Assignment of the possible cases defined in Figure 2 to the individual approaches of the framework.

3.1.1 Approach A: Two-step co-registration

According to the initial situation described above, the raw data for the analysis network consists of the as-planned BIM model and the as-built scan data in the form of a 3D point cloud. (Pătrăucean et al., 2015), who presented relevant work from the fields of computer vision, geometric processing, and civil engineering, claimed that the core of the as-built and as-planned comparison lies in the registration of the point cloud sampled from the as-planned BIM with the as-built point cloud. Therefore, we first followed the approach of aligning the data formats of the as-planned and as-built data by converting the as-planned BIM component into a mesh in order to create a point cloud with the points of the resulting vertices. For our study, an empirical evaluation showed that the mesh vertices provided sufficient density and no sparsity issues occurred. However, with regard to reproducibility and applicability to other datasets, upsampling can be considered by adding randomly selected points to the mesh to further increase the density.

On this basis, the two object point clouds are analyzed using a two-step co-registration process. First, a coarse registration is performed. This step is aimed at optimally pre-adjusting the objects in cases where there is significant rotation or displacement. To perform this coarse registration, we use the Fast Point Feature Histogram method as described in (Rusu et al., 2009).

Firstly, the relationships to its direct neighbors are calculated for each point in both point clouds, resulting in a simplified histogram (Simplified Point Feature Histogram, SPFH). Next, the SPFH is weighted with the SPFH values of the neighbors and merged to obtain a histogram (Fast Point Feature Histogram, FPFH), which summarizes the geometric relationships between a point and its neighbors and serves as a clear description of the local environment of a point. A schematic representation of this operation is shown in Figure 4. The figure shows how a point (red) is connected to its direct k-neighbors. Each direct neighbor is connected to its own neighbors and the resulting histograms are weighted with the histogram of the query point to form the FPFH. (Rusu et al., 2009)

CC BY

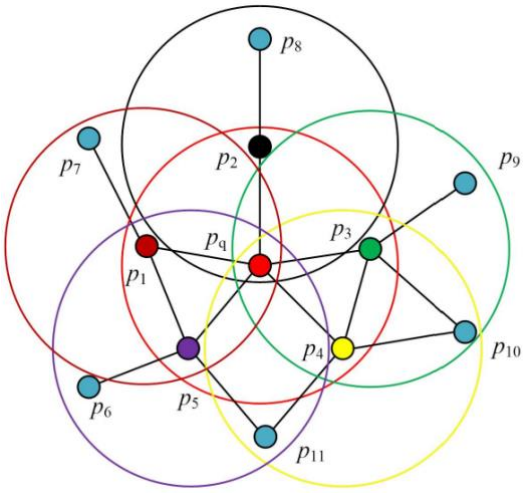


Figure 4: Areas of influence for creating Fast Feature Point Histograms (Xie et al., 2020).

Following the FPFH calculation, features of the points in both point clouds are compared in order to find possible point correspondences. For this purpose, FPFH values are checked for similarity. Meanwhile, points whose FPFH values are close to each other are considered potential correspondences. The identified correspondences can subsequently be used to estimate a transformation that aligns the two point clouds as closely as possible. In order of further improvement of the registration, the described coarse registration is followed by a fine registration using the method of Iterative Closest Point (ICP) (Besl & McKay, 1992; Zhang, 2021). Here, Point-to-Plane ICP is applied, which minimizes distances along surface normals rather than direct point-to-point distances, providing faster and more accurate convergence for structured or planar surfaces. Additionally, a multi-scale refinement is performed, where ICP is applied sequentially at decreasing voxel resolutions, optionally using a robust kernel to reduce the influence of outliers. This step further refines the transformation and ensures high alignment accuracy.

The result of the estimated transformations from the coarse and fine registrations is presented as a 4x4 transformation matrix A. This matrix comprises a rotation matrix r_{ij} and a translation vector t_{xyz} and is extended for 3D operations by employing homogeneous coordinates.

$$A = \begin{bmatrix} r_{11} & r_{12} & r_{13} & t_x \\ r_{21} & r_{22} & r_{23} & t_y \\ r_{31} & r_{32} & r_{33} & t_z \\ 0 & 0 & 0 & 1 \end{bmatrix} \tag{7}$$

The product of multiplying the transformation matrices obtained from the coarse and fine registrations yields a matrix that reflects the spatial relationship between the as-planned and as-built point clouds. From the rotation matrix and translation vector contained within this resultant matrix, it is thus possible to infer the extent to which the installed TBE component has been rotated or displaced. Ideally, the resulting transformation matrix A would be identical to the identity matrix I if the component were installed precisely according to the as-planned BIM. Consequently, for the automated evaluation of this approach, the difference matrix D between T and I is computed.

$$D = A - I \tag{8}$$

Subsequently, a hypothesis test in the form of a paired t-test (Witte et al., 2020) is conducted to determine whether the mean deviations of the difference matrix D are statistically significantly different from zero. The null hypothesis (H0) thus posits that the mean of the deviations in D is equal to zero. For this purpose, the mean value $\bar{d}$ (Equation 9) and the standard deviation s_d (Equation 10) of the total number n of the values d_{ij} in the difference matrix D are determined, followed by the calculation of the test statistic t (Equation 11).

$$\bar{d} = \frac{1}{n}\sum_{i=1}^{n} d_i \tag{9}$$

CC BY

$$s_d = \sqrt{\frac{1}{n-1}\sum_{i=1}^{n}(d_i - \bar{d})^2} \tag{10}$$

$$t = \frac{\bar{d}}{s_d / \sqrt{n}} \tag{11}$$

Next, the value of the test statistic t is used to determine the probability p from the t-distribution, which assesses the likelihood of the observed data to be occurring under the null hypothesis. The assertion that the TBE component is constructed in accordance with the as-planned data is accepted if the transformation matrix A does not statistically significantly differ from the identity matrix, thereby satisfying the condition

$$p > \propto \tag{12}$$

Otherwise, the null hypothesis is rejected if the following applies

$$p \leq \propto \tag{13}$$

If it is certain that the as-built and planning data pertain to the same TBE component, the transformation matrix resulting from the two-stage co-registration can also be used for the automated modeling of an as-is BIM model (Figure 5).

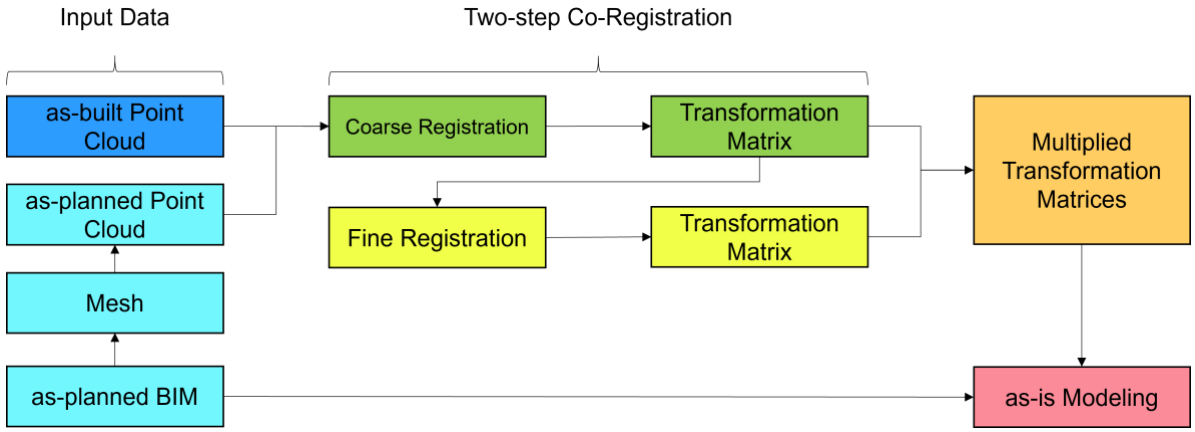


Figure 5: Conceptual Diagram of the Approach.

3.1.2 Approach B: Median-based Evaluation

Analogously to the technique presented in chapter 3.1.1, in the second approach we aim to perform a TBE component analysis based on identical data types for as-built and as-planned datasets represented as point clouds. The primary objective of our second approach was to determine the distances between the as-planned and as-built point clouds to gain insights into the alignment between planning data and real-world data. In the first phase, we aimed to calculate the distances between all points in the as-built point cloud and the as-planned point cloud. However, it is crucial to ensure that corresponding points from both point clouds are accurately matched. Otherwise, the analysis would not result in the actual distance between the point clouds, but rather the shortest possible distance. Figure 6 illustrates this with an example of a slightly displaced component.

To determine the corresponding point pairs, the two point clouds are aligned with each other using the registration method described in detail in chapter 3.1.1. Thereupon, the nearest neighbor is determined for each point of the as-built point cloud and its corresponding point in the as-planned point cloud is recorded. Subsequently, the actual distances between the two point clouds can be calculated in their original pre-registration positions using the logged point pairs.

In the next step, the median $\tilde{x}$ is determined from all distances between the corresponding point pairs of both point clouds. In this context, the median is more meaningful than the mean value $\bar{x}$ as it is less sensitive to outliers

CC BY

(Lehmann, 2023). In a point cloud, individual points can be significantly distanced from the majority of the data due to measurement errors or other disturbances, which would distort the mean value. The median, on the other hand, remains stable even if individual points (less than 50%) are widely spaced, providing a more robust measure of the central tendency of distances.

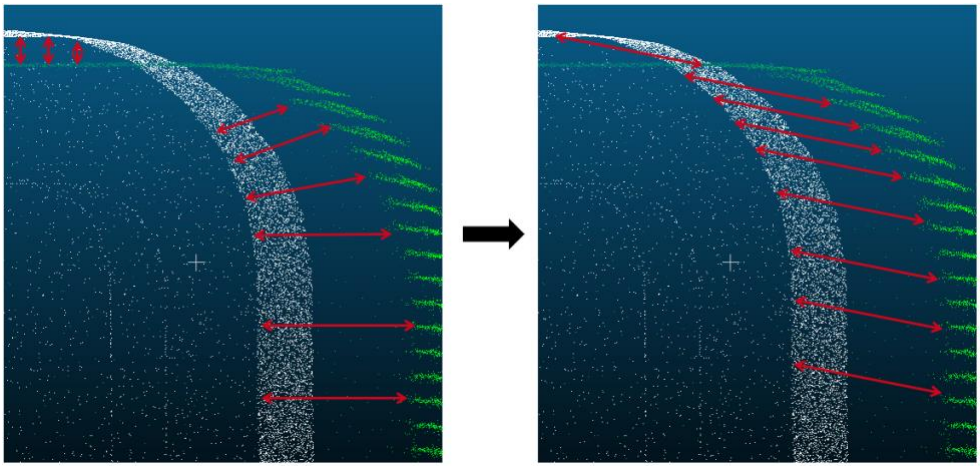


Figure 6: Illustration of the shortest distance calculation between two point clouds (left) and the determination of actual distances between corresponding point pairs (right).

However, since the generation of point clouds is always subject to a randomized point distribution, the distance between point pairs can only be zero by chance, even if the TBE component was installed precisely according to the planning specifications. For this reason, we decided to calculate the shortest distances between each point of the as-built point cloud and the mesh of the as-planned data instead of the distances between the point pairs. In this way, the confounding factor of the randomized point distribution of a point cloud is excluded, and a more precise analysis of the correspondence between the planned and actually implemented components is made possible.

For the automated classification of the TBE component, the determined median value is finally compared with the permissible tolerance threshold using the statistical evaluation method of a hypothesis test (Witte et al., 2020). Meanwhile, the null hypothesis (H0) asserts that the component was installed within the permitted construction tolerances and is confirmed if

$$\tilde{x} \leq \tau \tag{5}$$

applies. Conversely, the null hypothesis is rejected if

$$\tilde{x} > \tau \tag{6}$$

applies.

3.1.3 Approach C: Voxel-based Analysis

In a further approach, we pursued the goal of identifying component-specific sub-areas of the as-built data that do not significantly deviate from the as-planned data, considering the applicable tolerances. This was done to facilitate predictions regarding the classification of the respective TBE component, based on the identified overlapping sub-areas as well as the overall percentage distribution. A voxel-based approach was chosen for this, as voxel-based techniques have the advantage of speeding up processing and improving robustness to noise, occlusions and density variations (Martens & Blankenbach, 2023).

For the voxel-based analysis, both the as-planned point cloud of a component, generated as described in 3.1.1, and the corresponding segment of the as-built point cloud are transferred into a voxel grid. In this process, the multitude of points is aggregated based on the defined size of individual grid cells (voxels), creating the organized structure of a regular 3D grid. The level of detail of the 3D grid, and thus the resulting analysis, is significantly influenced by the chosen voxel size. Since the planned and realized states of the TBE components are to be evaluated taking into account a defined tolerance as described above, we have adapted the tolerance value determined according to Equation 4 as a voxel size in this approach. In this way, compliance with the specified tolerance can be ensured

CC BY

for overlapping voxels from the as-planned and as-built datasets. Subsequently, a neighborhood analysis identifies only the voxels within the voxel grid of the as-planned data that represent the surfaces of the components, while the remaining voxels are discarded. This step is essential because, during the voxelization of the components from the design model, the entire volume of the components is divided into voxels, whereas the as-built data only includes voxels located on the component surfaces. In this way, the voxel grids of the point clouds in the as-built and in the as-planned state can be directly compared, which are aligned in a uniform coordinate reference system according to the predefined initial situation. For each voxel in the as-built point cloud, it is checked whether there are overlaps with any voxel from the as-planned voxel grid, which leads to a corresponding categorization of each voxel. Figure 7 illustrates a visual example of the described voxel analysis.

As mentioned earlier, point clouds are inherently subject to random distribution, which also affects the automatically generated voxel grids. To address this issue, we refined the previously described method by voxelizing only the as-built point cloud instead of transforming both the as-built and the as-planned data into voxel grids. The resulting voxels are then checked for overlaps with the mesh of the as-planned component.

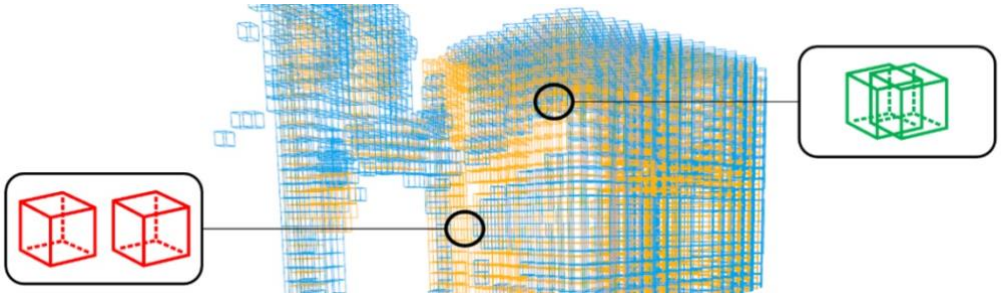


Figure 7: Voxel-based analysis of the as-planned (yellow) and as-built (blue) point cloud for voxel categorization as overlapping (green) or non-overlapping (red).

The results of the voxel-based analysis provide a detailed representation of reality. Not only do they enable the identification and visualization of overlapping and non-overlapping areas between the as-planned and as-built data, but they also form the basis for the classification of the TBE component. This classification is carried out by means of a subsequent statistical analysis and categorization of the entire voxel distribution. For this purpose, the number and percentage of overlapping voxels (p_O) and non-overlapping voxels (p_{NO}) is determined and then evaluated using predefined assumptions thresholds (γ_i) as exemplified in Table 1Table 1.

Table 1: Categorization of the voxel-based analysis results.

Analysis results	Assessment
$p_O \geq \gamma_1$:	The TBE component is assumed to be correctly installed
$\gamma_2 \leq p_O < \gamma_1$:	The TBE component may be rotated, displaced or a different component may have been installed
$p_O < \gamma_2$:	The TBE component is probably missing or displaced or another component has been installed

3.1.4 Approach D: Iterative Analysis of Convex Hulls

Our fourth method for analyzing as-planned versus as-built data of TBE components focuses on an iterative convex hull analysis of the respective point cloud data. Previous approaches yield results only for individual classification possibilities of the TBE components. In contrast, this method offers a holistic classification, enabling assignment to all categories illustrated in Figure 2. Consequently, the approach is designed to identify positional and structural deviations, enabling the detection of whether the constructed object conforms to its planned specifications or exhibits discrepancies, such as translation and rotation.

To initiate the process, the spatial extent of the as-planned an as-built point clouds is determined by identifying the minimum and maximum coordinates along the X, Y, and Z axes. Following that, the principal axis is identified by comparing the span of coordinates across each dimension in both datasets, selecting the dimension with the largest overall range. The identified principal axis serves as the directional reference for the following systematic segmentation of the as-planned and the as-built point clouds into cross-sectional slices, ensuring that the spatial

CC BY

orientation of each iteration is consistent. The thickness of each segment is controlled by an iteration size. The iteration size can either be calculated individually by dividing the maximum range of the principal axis by a specified number of iterations or set uniformly with a constant value. Within each iteration, all points that fall within the limit of the current slice are collected. This process of creating matching regions across both point clouds allows for a localized comparison, isolating changes within each segment independently.

For each segment in both point clouds, the algorithm constructs a convex hull by generating a triangular mesh that represents the surface and boundary of the slice. In order to detect structural deviations, the volume is then calculated and logged for both convex hulls of each iteration. In addition, the coordinates of the centroids of both convex hulls are determined and recorded. These centroids provide a center of mass for each segmented volume, which is key for identifying any spatial offset between the as-planned and as-built point clouds. An example of the data to be logged for each iteration step is visualized in Figure 8.

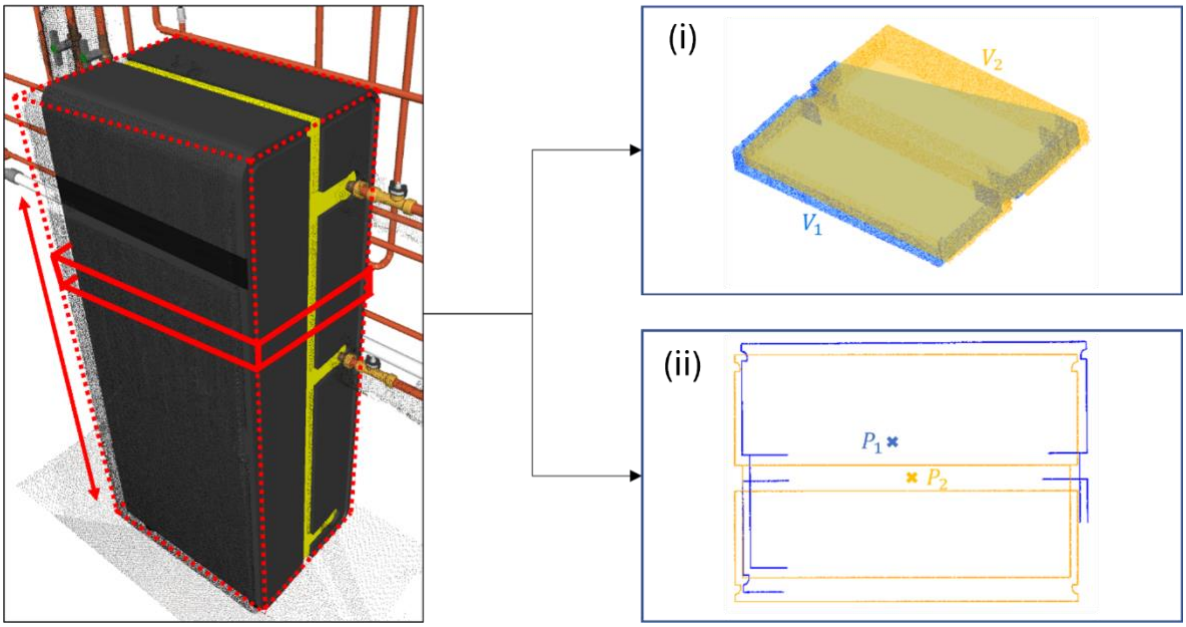


Figure 8: Exemplary iterative convex hull analysis of an as-planned point cloud (yellow) and an as-built point cloud (blue), with the convex hull volumes (V1, V2) shown in subfigure (i) and the centroids (P1, P2) illustrated in subfigure (ii).

All calculated volumes and centroid coordinates are then aggregated across each segment for both point clouds. This collection of data enables a robust comparison of corresponding geometric features, which can be used to reveal trends or anomalies. Significant differences in volume between corresponding segments, for instance, suggest inconsistencies in construction and potential structural mismatches, pointing to construction deviations from the planned specifications under the assumption of a low-occlusion acquisition of the as-built data. Shifts in centroid positions may indicate rotational or translational misalignments. More specific, linear shifts in centroid positions along the principal axis point toward translation, while non-linear shifts suggest rotational deviation.

Based on the aggregate results, two hypothesis tests are conducted to evaluate the conformity between as-planned and as-built data. The application of hypothesis tests in this approach follows the structure of a t-test. The initial hypothesis test assesses whether the differences in volume at each iteration step are statistically significant, serving as a method for detecting structural deviations. To account for the defined tolerances, any deviations falling below the tolerance threshold are rounded down to zero. The null hypothesis (H0) posits that the as-planned and as-built data are identical. Following the procedure outlined in 3.1.1, the probability (p-value) of the null hypothesis being true is subsequently calculated. The p-value is then compared against the established significance level, accepting the null hypothesis if Equation 12 is satisfied and rejecting it if Equation 13 applies. The second hypothesis test follows the same methodology as the first, with the distinction that it evaluates the differences in the XYZ coordinates of the centroids rather than volume discrepancies. This test is conducted individually for each axis to detect potential translational shifts.

CC BY

Finally, it needs to be checked if the as-planned and the as-built component are uniform in their basic geometry, even if they are dimensioned differently in both datasets. Such is often the case, for example, with pipes in the TBE that are planned without a corresponding covering in the course of the planning process, but are recorded with a covering in the course of reality capturing after the installation has been realized. In this case, the documented volumes of the iteratively determined volumes would differ greatly from each other, which would result in an incorrect categorization of the component by the automated method.

Therefore, we recorded the volumes of the as-planned and as-built component iterations in a diagram, with the iterations plotted on the x-axis and the volumes on the y-axis. The corresponding values were entered and connected linearly to create a graph. Subsequently, the as-planned and as-built volume graphs of a component are analyzed for similarity. This analysis examines whether the as-built volume graph increases in the same segments as the corresponding as-planned graph or exhibits an opposite trend. Specifically, the concept of a normalized cross-correlation is used for this purpose, which measures the similarity between two datasets as a function of a temporal shift (lag) (Hoffmann and Wolff, 2014). For this purpose, the linear correlation coefficient r between two discrete data series x_i and y_i is calculated by

$$r_{xy}(k) = \frac{\sum(x_i - \bar{x})(y_{i+k} - \bar{y})}{\sigma_x \sigma_y N} \tag{14}$$

(Hoffmann and Wolff, 2014; Witte et al., 2020) . In this case x_i and y_i are the volume values of the iterations of the as-planned and as-built components, k is the lag, $\bar{x}$ and $\bar{y}$ are the mean values of all respective volume values, σ_x and σ_y are the standard deviations of the volume values and N is the number of values considered. We then determine the lag with the largest linear correlation coefficient. The value of the resulting linear correlation coefficient serves as a measure of the linear dependence of the two data series and is always between the fixed limit values

$$-1 \leq r_{xy}(k) \leq 1. \tag{14b}$$

In this context, a resulting value of minus one or one stands for a strict linear dependence and a value of zero, on the contrary, has no stochastic linear dependence.

Due to the existing possibility of significant influence by outliers or scattering of the measurements, which can decisively influence the cross-correlation, we have previously applied a Savitzky-Golay filter (Savitzky & Golay, 1964) to the data in order to exclude such deviations. The Savitzky-Golay filter reduces the noise in the data while retaining important trends. This filter is based on a local polynomial fit of the data within a defined window and thus enables smoothing without distorting significant features of the original data. Mathematically, this means that a polynomial of a certain order is fitted for each pair of data points within a sliding window, whereby the coefficients of the polynomial are determined by weighted least squares fitting. Smoothing is performed according to the formula

$$y_i = \sum_{j=-m}^{m} c_j x_{i+j}\,, \tag{15}$$

where y_i is the smoothed value, x_{i+j} is the original values within the smoothing window, c_j is the coefficient of the polynomial fit and m is the half of the smoothing window (Chen et al., 2004; Savitzky & Golay, 1964). This ensures that short-term fluctuations in the data are minimized while the general structure of the data is preserved. The coefficients c_j are determined in such a way that the sum of squared errors is minimized

$$\begin{aligned} &min \sum_{i=-m}^{m} \left(x_i - P(i)\right)^2 \\ &with\ P(i) = \sum_{k=0}^{k} c_k i^k, \end{aligned} \tag{16}$$

CC BY

where $P(i)$ is the approximated polynomial (Savitzky & Golay, 1964). The application of the Savitzky-Golay filter thus contributes to improving the robustness of the normalized cross-correlation analysis by reducing systematic measurement deviations. As a result, the reliability of the determined correlations increases, which enables a more precise assessment of the similarity between the volume curves of the as-planned and as-built components.

For the classification of the TBE component, a threshold value λ is defined for the correlation factor, above which there is sufficient agreement between the volume graphs to assume that the corresponding as-planned component was installed in reality. In order to include correlation factors that deviate slightly from this threshold value, a hypothesis test is used to check whether correlation factors that are smaller than the defined threshold value λ actually deviate statistically from the threshold value. Therefore, the null hypothesis of the hypothesis test states that the actual correlation reaches or exceeds at least a specified threshold value. The alternative hypothesis postulates that the correlation is below this threshold value. As correlation factors for small sample sizes n_1 cannot assumed to be normally distributed, the Fisher Z-transformation (Fisher, 1915) is used for the hypothesis test with a probability of error φ, which first transforms the observed correlation r_{xy} into an approximately normally distributed variable z_1^* by the formula

$$z_1^* = \frac{1}{2} ln \frac{1 + r_{xy}}{1 - r_{xy}} \tag{17}$$

(Fisher, 1915; Witte et al., 2020). The standard deviation of the variable z_1^* can be estimated as

$$\sigma_{z_1^*} = \frac{1}{\sqrt{n_1 - 3}} \tag{18}$$

(Fisher, 1915; Witte et al., 2020). Similarly, the threshold value is also transformed by

$$z_0^* = \frac{1}{2} ln \frac{1 + \lambda}{1 - \lambda} \tag{19}$$

(Fisher, 1915; Witte et al., 2020). Finally, the standardized test statistic $\hat{z}$ can be calculated by

$$|\hat{z}| = \frac{|z_1^* - z_0^*|}{\sigma_{z_1^*}} \tag{20}$$

(Fisher, 1915; Witte et al., 2020). To decide whether to accept or reject the null hypothesis, the critical value of the standard normal distribution $z_{1-\frac{\varphi}{2}}$ must first be determined in relation to the selected probability of error φ. On this basis, the null hypothesis is accepted if

$$|\hat{z}| < z_{1-\frac{\varphi}{2}} \tag{21}$$

is fulfilled. By contrast, if

$$|\hat{z}| \geq z_{1-\frac{\varphi}{2}} \tag{22}$$

applies, the null hypothesis is rejected. Due to the increased level of complexity, the workflow of the approach presented is shown as pseudo code in Listing 1.

3.1.5 Combined classification framework

We previously introduced four different approaches for object-based geometric analysis of as-planned and as-built data of TBE components in combination with statistical hypothesis tests for automatic evaluation. For the final classification of the individual TBE components according to the categories defined in Figure 2, the individual approaches need to be merged into a combined classification framework.

CC BY

Listing 1: Pseudocode for the analysis of convex hulls.

```
function:  IterativeConvexHullAnalysis (P_plan, P_build, N): {D}
input:     P_plan    - As-planned Point Cloud
           P_build   - As-built Point Cloud
           N         - Number of Iterations
output:    D         - Classification Outcome

for P_plan, P_build do
    // Segmentation
    Determine principal_axis with maximal spatial extent
    Divide principal axis into N slices {S_1, ..., S_N}
    // Feature Extraction and Aggregation
    for each slice S_k do
        Compute Convex Hull
        Compute Volume
        Compute Centroid
    end-for each
end-for

// Statistical Evaluation
Calculate Volume Differences for all k
Calculate Centroid Differences for all k
ΔV_conf, ΔZ_conf ← Compute Confidence Interval
Perform hypothesis tests on ΔV_conf and ΔZ_conf

// Correlation Analysis
V_plan_smooth, V_build_smooth  ← Apply Savitzky Golay Filter
Compute Cross Correlation R between V_plan_smooth and V_build_smooth
R_norm ← Apply Fisher-Z-Transform to R
Evaluate significance of R_norm

// Classification
Determine classification outcome D based on statistical tests and correlation

return {D}
```

The first category for classifying the TBE components comprises the analytical result that the respective component was installed in reality according to the planning specifications (1A). This classification is made under some constraints. For approach A, the transformation matrix of the two-stage co-registration must not deviate significantly from the identity matrix. In the case of approach B, the median of the distances should show no significant deviation. Approach C requires that the proportion of overlapping voxels reaches at least the value of γ_1. Finally, in approach D, neither the volumes nor the differences and variances of the XYZ-coordinates of the centroids of the iteration steps may deviate significantly, taking the tolerance into account. In addition, the correlation factor of the volume graphs must be higher than the defined threshold value.

Conversely, a component is classified as rotated (1B) when a significant deviation is detected in Approaches A and B, while less than the value of γ_1 of all voxels are categorized as overlapping in Approach C. For Approach D, no deviation in the center coordinates is detected in this context, but there is a significant deviation in the volumes and a lower correlation factor in the volume graphs, as the defined threshold value is detected.

A component is classified as displaced (1C) when the criteria for Approaches A, B, and C align with those for the rotated category. In Approach D, however, significant deviations are found only for the centroid coordinates of the iterations, but no deviations in volumes, which also results in a higher correlation factor value than the defined threshold.

CC BY

Table 2: Classification framework combined by all approaches and their hypothesis tests.

			Component exists (1)				**Component does not exist (2)**	**Different component installed (3)**
			Not rotated or dis-placed (1A)	**Rotated (1B)**	**Displaced (1C)**	**Rotated and dis-placed (1D)**		
Approach A	T_1	$p > \propto$	True	False	False	False	False	False
		$p \leq \propto$	False	True	True	True	True	True
Approach B	T_2	$\tilde{x} \leq \tau$	True	False	False	False	False	True/ False
		$\tilde{x} > \tau$	False	True	True	True	True	True/ False
Approach C	T_3	$p_O \geq \gamma_1$	True	False	False	False	False	True/ False
		$\gamma_2 \leq p_O < \gamma_1$	False	True/ False	True/ False	True/ False	False	True/ False
		$p_O < \gamma_2$	False	True/ False	True/ False	True/ False	True	True/ False
Approach D	T_4	$p_{Vol} > \propto$	True	False	True	False	False	False
		$p_{Vol} \leq \propto$	False	True	False	True	True	True
	$T_{5,6,7}$	$p_{Diff} > \propto$	True	True	False	False	False	True/ False
		$p_{Diff} \leq \propto$	False	False	True	True	True	True/ False
	T_8	$r_{xy}(k) \geq \lambda$	True (False)	False	True (False)	False	False	False
		$r_{xy}(k) < \lambda$	False (True)	True	False (True)	True	True	True
	T_9	$\lvert\hat{z}\rvert < z_{1-\frac{\varphi}{2}}$	True	False	True	False	False	False
		$\lvert\hat{z}\rvert \geq z_{1-\frac{\varphi}{2}}$	False	True	False	True	True	True

A combination of rotation and translation (1D) is identified when significant deviations are found in each of Approaches A, B, and D, and Approach C shows that the proportion of overlapping voxels in the total voxel grid is less than the value of γ_1. If a component from the planning model is missing in reality, this is indicated either by the inability to perform the analyses due to a completely absent as-built dataset or by an overlap percentage of less than the value of γ_2 in Approach C, combined with significant deviations in the respective evaluation metrics across all other approaches.

CC BY

The scenario in which a component differing from the planning model is installed in its place (3) cannot be clearly identified by this type of analysis, as also shown by related publications above. The diverse geometric characteristics and the uncertainty regarding the orientation of the differing component preclude the assumption of significant deviations across various tests in an automated analysis. Nevertheless, in such cases, it is anticipated that Approach A will produce a transformation matrix that significantly deviates from the identity matrix, while Approach D will reveal a volume difference during the iterative steps. For other analytical approaches, no conclusive observations can be made. Consequently, this scenario cannot be clearly distinguished from other classifications, particularly the "Rotated and Displaced" category, and must always be considered as a potential outcome. The outlined decision-making framework is summarized in Table 2.

In summary, this methodology provides a systematic, segment-wise comparison between the as-planned and as-built models, supporting precise quality assurance by revealing positional and structural discrepancies. This process ensures that any deviation, whether a minor misalignment or a major structural inconsistency, can be detected, quantified, and visualized, providing critical insights into the accuracy of construction in relation to planned designs. Based on these results, the TBE system can be divided into areas where the methodology can reliably identify either a match or a validated discrepancy between the as-planned and the as-built data, and areas where no valid statement can be made and manual verification is therefore required. Furthermore, the methodology presented forms a fundamental benefit for the generation of DTw, provided that the specified initial situation is adhered to and, in particular, an as-built detection with limited occlusion is achieved.

4. IMPLEMENTATION

In this chapter, the practical implementation of the methodology described above is presented. First, we introduce the datasets on which the methodology was applied. Next, we outline the implementation in detail, including the technical application and the selected parameter values.

4.1 Datasets

For the initial performance analysis of the proposed method, a manually generated simulated dataset with simple geometric shapes was created. Using the BIM authoring software Autodesk Revit[2], a simple geometric model was constructed, consisting of a wall and a column, both represented as cuboids (Figure 9). Those objects were selected to verify that the method performs well for simple geometric shapes before applying it on complex geometries of TBE systems. Each object was then modified by controlled rotations, translations, or a combination of both. Uniform translations of one meter were applied, while rotations of 45° were performed on the column and 20° on the wall. These transformation parameters were selected randomly, ensuring that the resulting spatial change was significant. To establish the required baseline conditions all modeled objects were first converted into meshes and then transformed into object point clouds, which served as as-built data. To ensure a realistic representation, the point clouds were also augmented with a noise factor of 5 mm, corresponding to the accuracy of the geodetic terrestrial laser scanner Riegl VZ-400i used for the other datasets, as specified by the manufacturer (Riegl, 2017). This enabled the simulation of various scenarios for the wall and the column, including cases where the objects were realized without deviation and where rotations or translations were introduced. To simulate the case where an object was absent, an empty point cloud was used as the as-built data. A further scenario involved the installation of an incorrect component, represented by using the wall object as the as-planned dataset and the column object as the as-built dataset. During the manual creation of this dataset, care was taken to exclude potential sources of interference, such as occlusions in the point clouds representing the as-built data. In this way, it was ensured that the analysis methods could be validated under idealized conditions, focusing solely on their fundamental functionality.

The second dataset consists of a physical TBE demonstrator designed to represent typical TBE geometries. The structure includes eleven components made up of plastic pipes, cuboid and cylindrical elements simulating TBE components, as well as metal pipes. The demonstrator has a width of approximately 1 m, a height of 1.5 m, and a depth of 0.4 m. It was suspended from the ceiling using nylon threads and stabilized with weights on the floor to

[2] https://www.autodesk.com/products/revit/

CC BY

minimize movement during the scanning process. The data was collected under controlled laboratory conditions using again the Riegl VZ-400i laser scanner with an accuracy of 5 mm. The scanning process covered 360 degrees from multiple heights to prevent occlusions. In addition, obvious outliers were removed by means of manual post-processing, whereby points located in empty space around the objects were roughly cropped. However, only points that could clearly distort the analysis were removed, while noise on the object surfaces remained unchanged. Based on the resulting point cloud, a digital model of the demonstrator was manually modeled to accurately reflect the real structure. To evaluate the methodology's ability to detect deviations, a second version of the digital model was manually modified. In this manipulated model, individual components were shifted by 20 centimeters, rotated by 35 degrees as well as rotated and shifted with the same values. In addition, one component representation was removed from the as-built point cloud (Figure 10). This dataset serves as a functional test for the methodology in a physical environment under laboratory conditions. The demonstrator includes TBE-relevant geometries and surfaces, and the scanning setup ensured a complete, occlusion-free acquisition. By applying the methodology to both the unmodified and the manipulated model, the dataset enables an evaluation of its performance on a real-world structure while minimizing external disturbances.

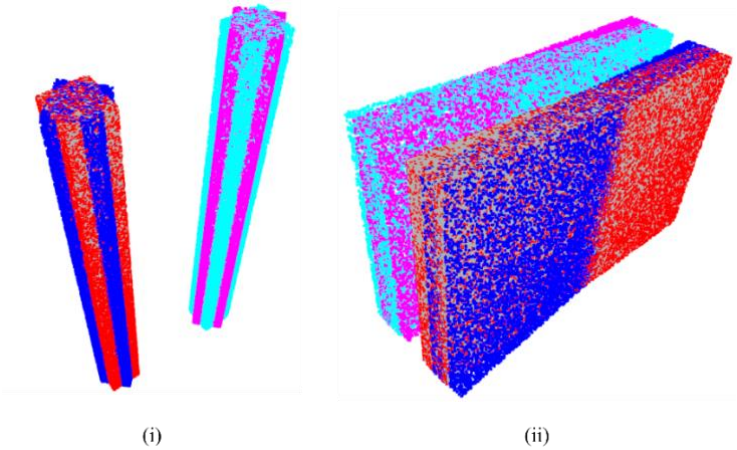


Figure 9: Point clouds of the simulated dataset showing (i) a column (0.5 × 0.5 × 3.0 m) and (ii) a wall (5.0 × 0.2 × 3.0 m), each illustrated in its original position (red), rotated (blue), displaced (turquoise), and rotated and displaced (pink).

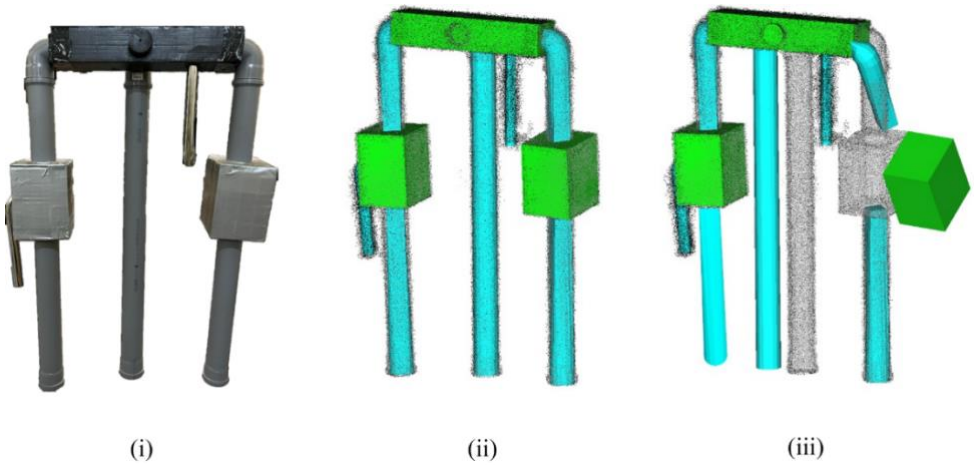


Figure 10: TBE demonstrator (i) and the non-manipulated (ii) and manipulated (iii) digital model with overlaid point cloud.

Finally, the third dataset consisted of a real technical installation located within a large hall, which was captured using TLS. More specifically, the data acquisition was again performed with the laser scanner Riegl VZ-400i from 45 scanning positions, which were subsequently registered into a single as-built point cloud. The registration of

the 45 scan positions was performed using a MultiStation Adjustment in RiSCAN Pro[3], utilizing a total of 961,308 plane patches. The resulting standard deviation of the residual distances between corresponding plane patches was 7.6 mm. Although the scans were planned to minimize occlusions, this could not be fully achieved due to the dense arrangement of the components. The resulting colored as-built point cloud of the dataset is shown in the appendix in Figure A1. The technical installation comprises a wide variety of 315 objects with complex geometries, including pumps, pipes, valves, control cabinets, and a steel framework. Pipes, for example, show high complexity due to different categories, varying diameters, long and slender runs, non-standard layouts, and interactions with surrounding components. A detailed representation of the included component types of the dataset is illustrated in Table A1 in the appendix. Consequently, the dataset represents diverse geometric forms and scales that characterize intricate TBE systems. Based on the resulting point cloud, the installation was initially reconstructed through a detailed manual modeling process (Figure 11). Each object was modeled directly from the point cloud data, capturing its geometry with as much detail and accuracy as the data allowed, so that the anticipated outcome of applying our analysis method to this dataset was the identification of all components as neither displaced nor rotated. This allowed for the evaluation of the method's functionality under real-world conditions, given the wide range of geometric forms and variations present within the components. The point cloud for this dataset was not manually refined, preserving the inherent characteristics of point clouds generated via laser scanning techniques. As a result, the dataset included noise and residual occlusions. These challenges are typical of point clouds obtained from laser scanning in the context of TBE systems. Specifically, laser scanning often leads to multiple reflections due to the numerous metallic surfaces of the components. Additionally, the complex structure and dense arrangement of TBE systems make it impossible to capture them entirely without occlusions. This dataset was therefore instrumental in testing the method's robustness and effectiveness in handling realistic data with typical imperfections arising from laser scanning processes.

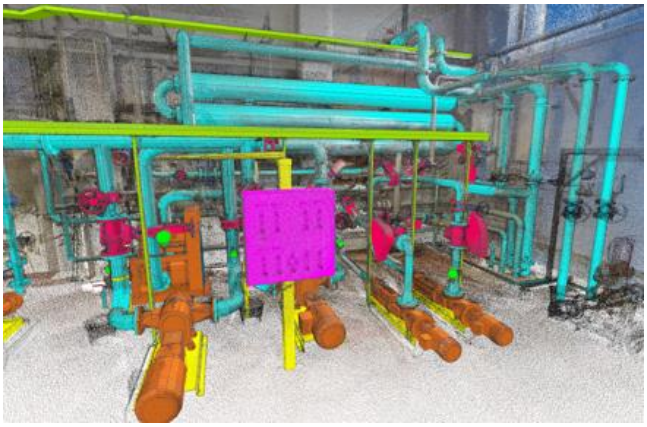


Figure 11: Dataset of a Field2BIM project.

4.2 Technical Implementation

For the technical implementation of the methodology, the as-planned and as-built BIM models were exported to IFC and converted into geometric mesh representations using the open-source library IfcOpenShell[4]. Each IFC element was meshed using IfcOpenShell's standard BRep triangulation, whereby world coordinates were used to ensure consistent positioning. The resulting meshes consist of vertices and triangular faces that represent the geometry of the elements. For further conversion into a point cloud, the mesh surfaces were uniformly sampled using the open-source library Open3D[5]. The number of points per triangular face was selected proportionally to its area, resulting in an even distribution of points across the surface. The total number of points per element was set at one million in order to capture sufficient geometric detail. To approximate measurement uncertainty, additive

[3] https://www.riegl.com/products/detail/riscan-pro

[4] https://ifcopenshell.org/

[5] https://www.open3d.org/

CC BY

Gaussian noise was applied to the point cloud, modeled as isotropic and independently distributed in all spatial directions, with a standard deviation corresponding to the specified measurement precision of the Riegl VZ-400i laser scanner. Following this, the generation of convex hulls could be generated using the open-source library SciPy[6].

As mentioned above, the tolerances, including the execution tolerance, which serve as the basis for the analysis, are usually specified in advance by the client or in accordance with applicable standards and guidelines in practice. Based on those defined values, it is the task of the surveyor, for example, to select a suitable measuring instrument in order to comply with these tolerances. Here, in order to be able to evaluate our methodology in practice, we defined realistic tolerances ourselves in order to use these values to check how our methodology performs under those conditions. Also, we defined all necessary thresholds by either empirically evaluated values or common application values. On the one hand, we have defined a tolerance value of 0.10 m for the execution tolerance τ_c. On the other hand, for the measurement tolerance τ_m, a standard deviation σ_m of 0.005 m results from the manufacturer's specifications of the TLS used. However, since the observed standard deviation of the residual distances after registration was 0.0076 m for the real-world dataset, we adopted a more realistic standard deviation σ_m of 0.008 m. To take account of unknown systematic measurement deviations, we have set the value of Δ_u to 0.01 m. According to Equation 3, this results in a measurement tolerance of 0.05 m. Hence, the total tolerance τ_{total} results in a value of 0.1118 m according to Equation 4.

Further to implement our methodology practically we defined a common α-value of 5% for the hypothesis test that determine whether the obtained transformation matrix significantly deviates from the identity matrix in Approach A.

In Approach C the threshold γ_1, which defines the percentage distribution of overlapping voxels beyond which the TBE component is assumed to be correctly installed, was set at 80%. Conversely, the threshold γ_2, beyond which it is assumed that the TBE component is probably missing, displaced, or replaced by another component, was set at 20%.

The number of iterations for the iterative analysis of convex hulls in Approach D was set to 50 in order to ensure a robust approximated normal distribution of the correlation factors within the Fisher-Z transformation. However,

before conducting statistical assessments, a preprocessing step was applied in which the 20% of the distribution of the XYZ-coordinates of the centroids with the highest deviation was identified and excluded to mitigate the influence of outliers. The same exclusion criterion was applied to the analysis of volume differences and cross-correlation, ensuring that the remaining 80% of the distribution formed the basis for further analysis. In the subsequent t-tests on the distributions of the recorded XYZ-coordinate differences of the centroids as well as on the volume differences across iterations, we again set the α-value to 5%. For the classification of components based on cross-correlation, the threshold λ for the resulting correlation factor, beyond which as-planned and as-built components are considered identical, was set at 0.8. Finally, for the Fisher-Z transformation, an error probability φ of 5% was chosen, yielding a critical value $z_{1-\frac{\varphi}{2}}$ of 1.96 for the standard normal distribution.

5. EVALUATION

For the evaluation of our automated and geometry-based analysis method for the comparison of as-planned and as-built data in the context of TBE systems for component-specific validation using statistical test procedures, various datasets were considered. The datasets differ in the degree of their potential confounding factors, allowing the basic functionality to be evaluated, possible application limits and result-distorting factors to be identified and optimization potential to be recognized. This section presents the results obtained on the various datasets with increasing complexity.

[6] https://scipy.org/

CC BY

5.1 Simulated dataset

The application of the proposed analysis framework to the simulated test dataset demonstrated the effectiveness of the method in various scenarios. For components where as-built data matched the as-planned specifications, the calculated median of the shortest distances between the as-built point cloud and the as-planned component was negligible and therefore below the tolerance threshold, indicating compliance with the design. The two-stage co-registration process resulted in a transformation matrix that deviated slightly from the identity matrix due to the iterative optimization process. However, the marginal deviations did not prove to be significant in the subsequent hypothesis test. As expected, the voxel-based analysis revealed a complete overlap, while the convex hull analysis revealed no significant differences in centroid coordinates or volumetric differences. Consequently, the cross-correlation analysis also resulted in higher correlation factors than the defined threshold value of 0.8, so that the components were correctly identified as installed according to design specifications.

When the as-built component was rotated relative to the as-planned BIM, the median distance exceeded the tolerance threshold. Furthermore, the transformation matrix derived from the co-registration significantly deviated from the identity matrix. The results of the voxel overlap, on the other hand, varied for the two different test objects. For the wall, the proportion of voxels with an overlap of the mesh of the as-planned data was in the range between 20 % and 80 %, while for the column it was over 80 %. The convex hull analysis detected no deviations in centroid coordinates for either component. However, the volumetric analysis revealed discrepancies for the wall along its representative axis, leading to a lower correlation factor of the cross-correlation analysis, which correctly classified the wall as rotated. In contrast, no volumetric deviations have been detected for the column along its representative axis, resulting in its misclassification as correctly installed. This highlighted a limitation of the method, where rotation is only detected when it does not occur along the analyzed axis.

For the components that have been translated, the median of the calculated distances also exceeded the tolerance threshold. Similarly, the transformation matrix resulting from the registration process again deviated significantly from the identity matrix, as the part of the translation vector in particular exhibited a corresponding characteristic. Furthermore, no overlap was detected in the voxel-based analysis, as anticipated. Nevertheless, the iterative convex hull analysis identified deviations for the centroids coordinates without volumetric anomalies. In this way, the component was correctly identified as being translated without any rotation.

In the cases where the components were both rotated and translated, all metrics investigated showed significant deviations. The difference with the results for the components that were only translated lies in the iterative analysis of the convex hulls, where significant deviations were found in the center coordinates and volumes. As a result, the components were either correctly identified as rotated and shifted or as potentially incorrect components. However, distinguishing between these two possibilities required remains a central issue as also shown by related works in this field (see Chapter 2). Therefore, in such cases manual inspection is unavoidable.

Proof of this could also be provided using the scenario of an installation of a component deviating from the planning situation. This case was simulated by using the wall in its initial position as an as-planned component and the object point cloud of the column as an as-built component. The result showed that all null hypotheses of the hypothesis tests and threshold comparisons applied to the results of the four different analysis methods were rejected for this example. With this result, the object could be identified as invalid. However, the obtained result data does not allow a precise distinction to be made as to whether a deviating component has been installed or whether the component is severely rotated and displaced. However, the algorithm enables pre-filtering in these cases. Table 3 summarizes the results of the method on the simulated dataset.

Table 3: Component analysis results for the simulated dataset.

Achieved classification	Wall	Column
Correctly Installed (1A)	True	True
Rotated (1B)	True	False
Displaced (1C)	True	True
Displaced and Rotated (1D)	True	True
Different component (3)	True /False	

In summary, the results from the test dataset confirmed the robustness of the method in identifying components installed according to design specifications or those subjected to translation. Rotations were reliably detected when

CC BY

convex hull analyses were extended to all axes. However, distinguishing between cases that combine rotation and translation and those where a deviating component has been installed remains a challenge.

5.2 TBE demonstrator

Our method was applied to the TBE demonstrator to evaluate its functionality using a real dataset under controlled conditions. As described in Section 4.1, the demonstrator was manually modeled both as a faithful representation of reality and with manipulated components that deviated from the actual structure.

In the first case, where the non-manipulated model was used as the as-planned BIM, the method correctly classified 9 out of the 11 components as identically installed. The components not classified as identical were the two metal pipes with polished surfaces. Since the scanning process of the TBE demonstrator was conducted in a near-range setup, the representations of these metal pipes in the point cloud were significantly affected by strong scattering due to multiple reflections. This pronounced scattering of measurement points led to discrepancies in the component analysis, as in Approach D the convex hull of the as-built point cloud exhibited substantial deviations from the convex hull of the as-planned component. Consequently, significant differences in volume metrics were observed, and the cross-correlation analysis revealed a low correlation factor. This finding indicates that the well-known problem of multiple reflections has a significant impact on the performance of our method, as also reported in related work. However, since the high occurrence of multiple reflections in this specific case is greatly increased by near-range scanning, it cannot be generalized that the method is unsuitable for components with metallic surfaces. The applicability of the method to such components under different scanning conditions is further analyzed in Section 5.3. To assess the results, Figure 12 presents the confusion matrix of the classification results together with the derived evaluation metrics accuracy, precision, recall and specificity. In this context, true positives (TP) refer to components that were correctly recognized as identically installed. False negatives (FN) denote components that were not recognized as identical despite being correctly installed. Since in this scenario only correctly installed components were evaluated, the categories true negatives (TN) and false positives (FP) remain empty.

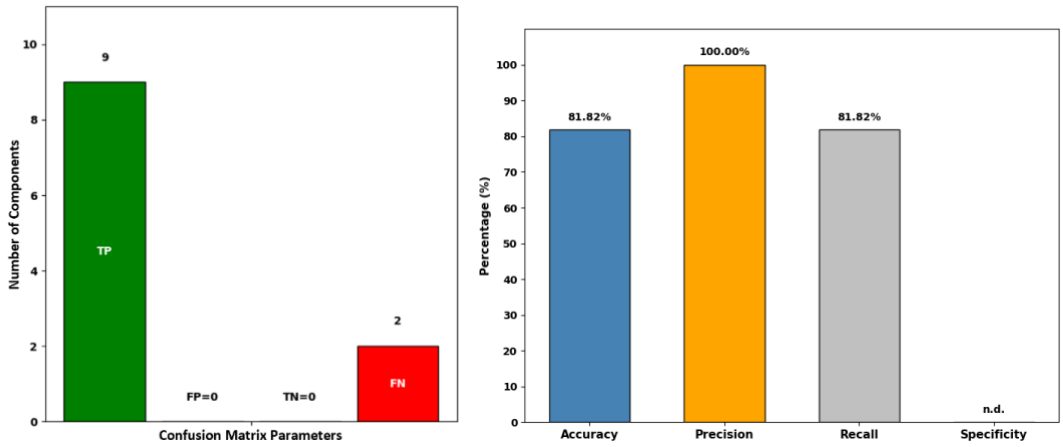


Figure 12: Summary of the TBE demonstrator results using the non-manipulated model, showing the confusion matrix parameters (left) and the derived evaluation metrics (right).

For the second use case of the demonstrator, the manipulated model, in which one component was each manually rotated, shifted, rotated and shifted as well as removed, was used as an as-planned BIM. In this case, the same results were obtained for the remaining non-manipulated components of the demonstrator as before, meaning that the two metal pipes were classified as not identically installed and the remaining components were classified as identically installed. The component whose representation was removed from the as-built point cloud to illustrate the possible case of a missing component in reality was in fact categorized as a missing or different component by the method. Through the object-based point cloud segmentation, only outliers and a small number of points of the neighboring elements were included in the analysis. As a result, the transformation matrix determined in Approach A deviated from the identity matrix and the median determined in Approach B deviated significantly from the

CC BY

defined tolerance limit. Similarly, in Approach C only a marginal number of overlapping voxels could be determined and in Approach D both the volumes and the centers differed significantly from each other. The components of the manipulated dataset that were rotated and the component that was shifted could also be correctly classified by the method. In both cases, the transformation matrix determined in approach A deviated significantly from the identity matrix, the median determined in approach B significantly exceeded the tolerance limit and the determined proportion of overlapping voxels in approach C was below the defined threshold γ_1. For the rotated component in approach D, on the other hand, a significant deviation of the volume differences and a low correlation factor of the cross-correlation analysis were diagnosed, but no significant deviation of the centroid coordinates. In contrast, for the shifted component, a significant deviation of the centroid coordinates, but no significant deviation of the volume differences, as well as a higher correlation factor than the defined threshold value λ was determined. Finally, in the analysis of the rotated and shifted component, all hypothesis tests of Approaches A, B and D were rejected. In Approach C a proportion of overlapping voxels between the threshold values γ_1 and γ_2 was determined. Thus, this component could also be correctly classified as either rotated and shifted or as another component. Figure 13 and Figure 14 summarize the results of the method on the manipulated TBE demonstrator dataset.

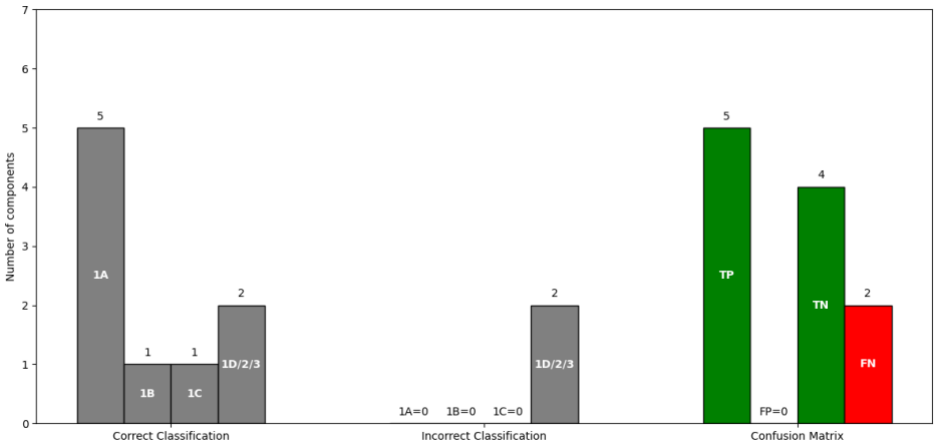


Figure 13: Classification results and resulting confusion matrix parameters for the manipulated TBE demonstrator.

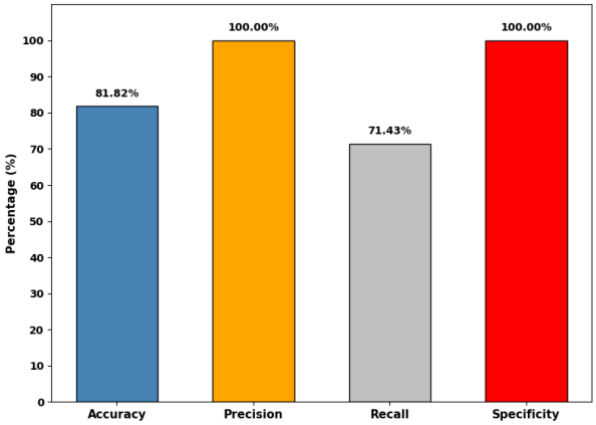


Figure 14: Evaluation metrics for the manipulated TBE demonstrator derived from the confusion matrix parameters of Figure 13.

Overall, the results obtained on the demonstrator with the non-manipulated and the manipulated digital model demonstrated the basic functionality of our method on a real dataset as long as the central requirement of sufficient scan data quality for geometry-based methods is fulfilled.

CC BY

5.3 Real-world dataset

The decision-making framework for component-specific comparisons of as-planned and as-built data for TBE systems was further evaluated using a real-world dataset in which the as-planned BIM model had been manually modeled based on the as-built point cloud.
By including unprocessed point cloud data with inherent noise, such as occlusions and multi-path reflections, this approach allowed us to assess the framework's robustness under realistic and imperfect conditions. In addition, this procedure enables the identification of limitations and areas for optimization.
The dataset includes 315 TBE components, with dimensions ranging from small-scale elements in the lower tens of centimeters to large-scale components spanning several meters. The holistic application of our method to the present dataset indicates that 195 out of a total of 315 components were identified as correctly installed, which corresponds to a reduction in manual effort for system verification of approximately 61.90%. However, 120 components of the dataset remain that were not classified as identical components by our method as expected. Figure 15 summarizes the results of the holistic approach of our method on the dataset.

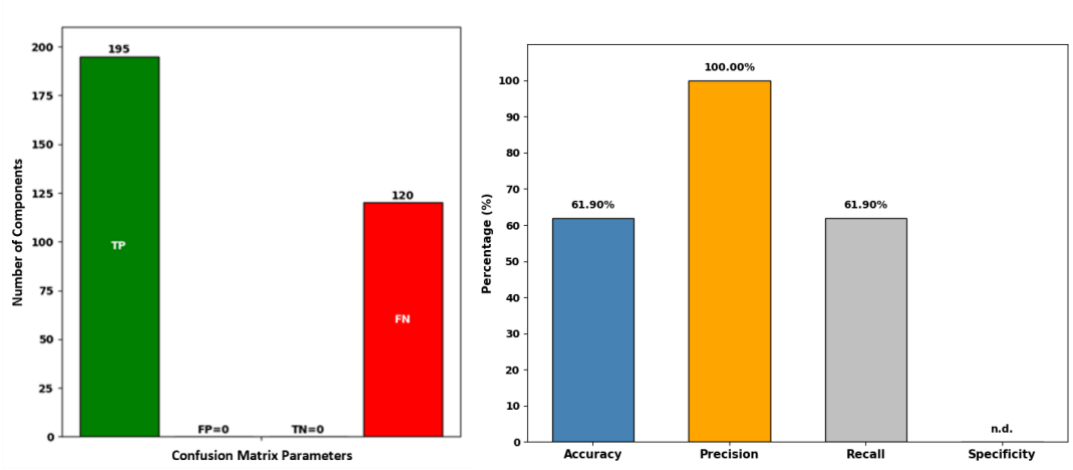


Figure 15: Summary of the real-world dataset results, showing the confusion matrix parameters (left) and the derived evaluation metrics (right).

A closer examination of the results obtained showed that in particular components that have not been affected by occlusions or surrounded by closely packed neighboring elements were consistently classified as matching the as-planned specifications without deviations. Due to the densely installed structure of the TBE system, this particularly affects the large proportion of the dataset of components that were directly accessible. In these scenarios, the object-based point cloud segmentation reliably captured the component's geometry, allowing the subsequent analytical methods to perform effectively due to the high overall data quality. An example of such a component is shown in Figure 16 in its initial position as well as in the course of the resulting object-based point cloud segmentation and the performed voxel-based analysis. Additionally, Figure 17 includes a graphical representation of the recorded XYZ centroid coordinates and volumes over the iterations performed as part of the convex hull analysis for the example component shown in Figure 16. The graphs demonstrate that while the method of iterative convex hull analysis is sensitive to outliers in the point cloud segments, the relatively low frequency and magnitude of such noise in these cases allow for a robust identification of the structural equivalence between as-planned and as-built data.

CC BY

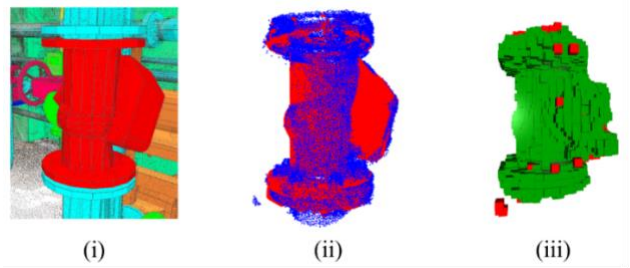


Figure 16: Properly detected TBE component in its initial position (i), segmented object point cloud (blue) overlaid with the as-planned mesh (red) (ii), and voxel-based analysis (iii) showing overlapping (green) and non-overlapping (red) voxels.

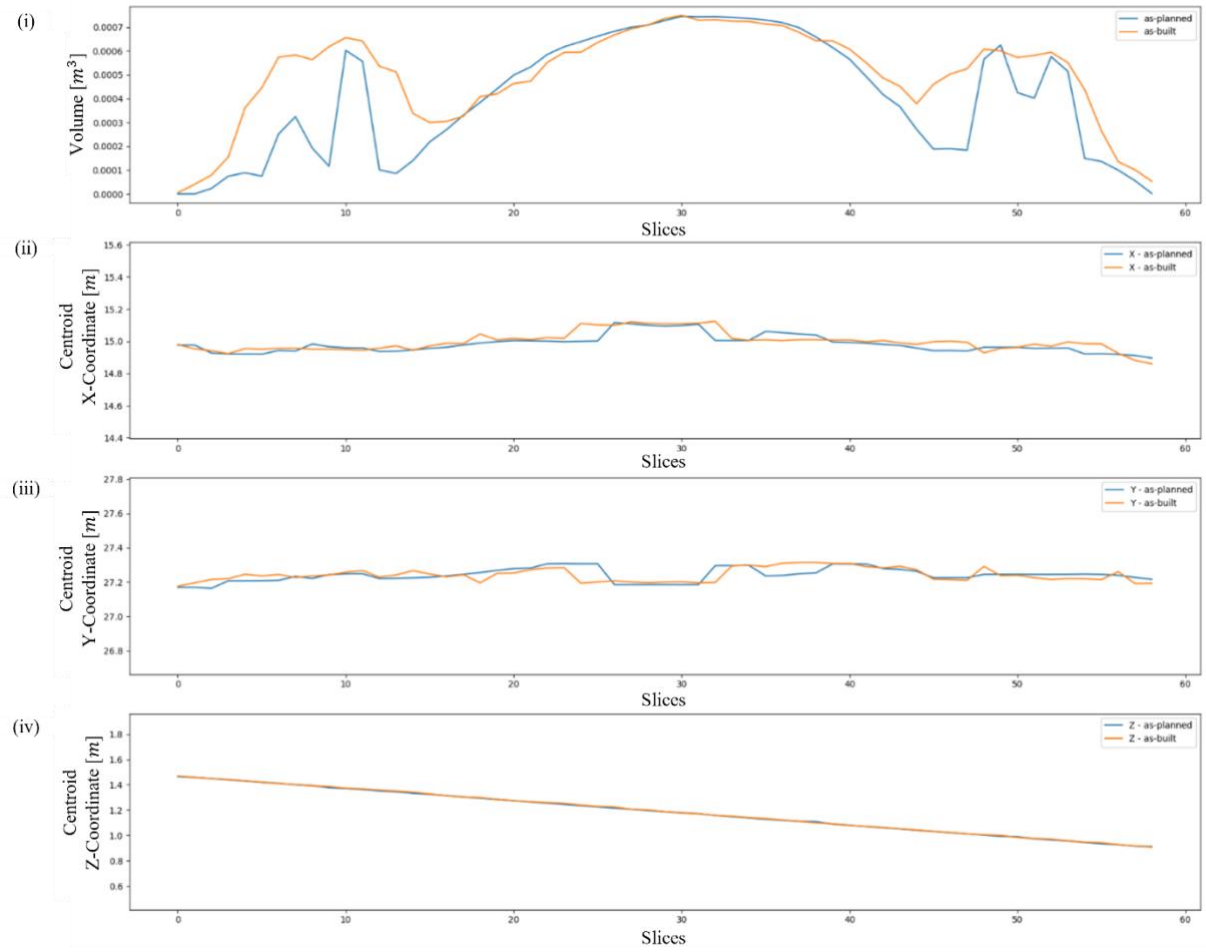


Figure 17: Convex analysis results for the TBE component shown in Figure 16.

On the other hand, the components that led to incorrect classification by our automatic analysis framework were those with a high degree of occlusion or very densely built-up neighboring components, which are partially included in the analysis as a result of the object-based point cloud segmentation and distort the result. In particular, components that are installed directly at the walls are affected by this, as it is not possible to capture such components in their entirety in the scanning process. The sum of these components represents a significant proportion of the dataset. Due to the missing parts of the geometric representation of these components in the as-built point cloud, our geometric analysis consequently reveals deviations between the as-planned and as-built data. The voxel-based approach is the only method that offers greater robustness against occlusions during geometry-based analysis. However, it does not make sense to rely exclusively on the results of this approach for classification.

CC BY

Therefore, as in other related work, the disruptive factor of occlusion cannot be compensated for by applying our methodology. In contrast, we have compensated for the interference factor of the partial inclusion of nearby neighboring elements by integrating the entire content of the as-planned BIM that lies within the bounding box of a component into the analysis. However, this compensation is only possible to the extent that the elements that are represented in the as-built point cloud apart from the actual object under investigation are also present in the as-planned BIM.

Another finding of the results analysis is that large-scale components are more often misclassified, whereas small-scale components are more often correctly classified. This fact can partially be explained by the fact that the degree of integration of other objects apart from the component under investigation increases with the larger size of the respective component. As a result, the risk of misclassification also increases, as more outliers of the point cloud are included in the analysis. Furthermore, significant deviations of neighboring components can also influence the classification depending on the degree of their integration into the analysis by the object-based point cloud segmentation. Figure 18 shows a corresponding example of such a case and its point cloud segmentation in superposition with the optimized as-planned mesh generation as well as the resulting voxel analysis.

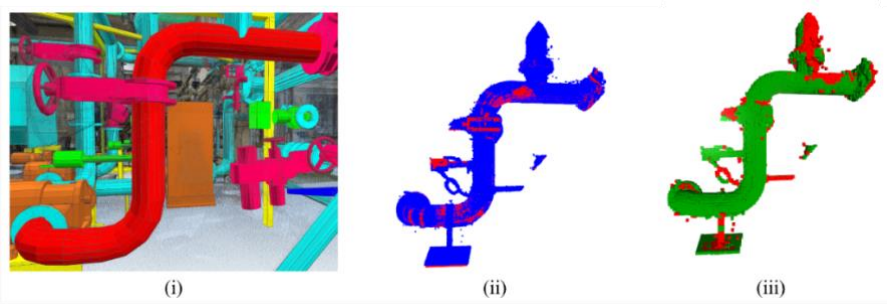


Figure 18: Complex TBE component in a densely built-up area in its initial position (i), segmented object point cloud (blue) overlaid with the optimized as-planned mesh (red) (ii), and voxel-based analysis (iii) showing overlapping (green) and non-overlapping (red) voxels.

To verify whether the method can be applied in practice to a real dataset with an imperfect point cloud, a subset of the TBE system was isolated from the center of the room. This test was carried out to evaluate the method`s performance on a real world dataset without being affected by the previously identified limitation regarding the integration of wall-mounted components that are only partially captured during the scanning process. This subset comprises 81 components, to which the method was applied again. The results of this second study show a significant improvement in the correct classification of the TBE components. Of the 81 components, 72 (88.89%) were reliably classified as correctly installed by the method, which confirms its functionality and effectiveness. Compared to the holistic approach, the correct classification rate was thus increased by 26.99%. A summary of the analysis results is shown below in Figure 19.

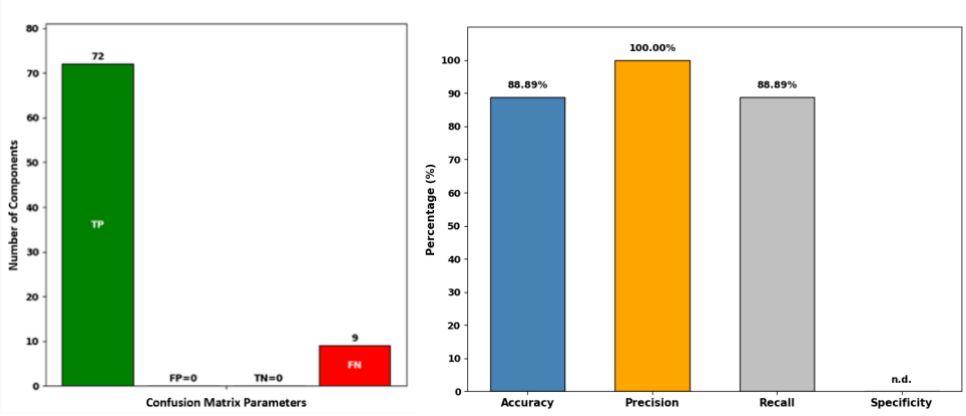


Figure 19: Summary of the results for the subset of the real-world dataset, showing the confusion matrix parameters (left) and the derived evaluation metrics (right).

6. CONCLUSIONS AND OUTLOOK

We have presented an automated decision-making framework for the comparison of as-planned and as-built data for TBE components. TBE systems pose a major challenge due to their complex geometries and densely built structures, which often lead to limited accessibility. The framework applies four consecutive geometry-based analyses combined with threshold comparisons and statistical evaluation methods to classify components as identically installed, rotated, displaced, both rotated and displaced, missing or replaced by another component. By evaluating the application of our method on various datasets with different geometric complexities of the TBE systems, scales and numbers of potential interfering factors, we examined the strengths and limitations of the presented methodology.

As a result, the technical functionality of the individual analysis methods and their practical benefits have been proven. If a sufficient scan quality is given, the method reliably identifies identically installed, rotated, and or displaced components. Under those conditions, a correct identification rate of over 88% was achieved on a real-world dataset. This leads to a significant reduction in manual effort, as the inspection process is transformed from a complete system check to a targeted validation of the remaining 12% of deviating or unclear cases. This optimization not only improves time and cost efficiency but also highlights the method's potential to support the creation of DTw within the complex environment of TBE systems. However, the aim of this study was not to develop a fully automated workflow for the entire TBE system, but to provide a practical tool to support the inspection process. By increasing the degree of automation, the method enables an initial classification of objects in terms of their spatial conformity with the planning data. Thereby, a distinction is made between components that can be evaluated with a high degree of certainty and those for which automated suggestions are available but still need to be validated manually.

An unavoidable limitation lies in the strong dependence on the quality of the input data, such as the Level of Detail (LOD) of the as-planned BIM. Furthermore, environmental factors like occlusions, noise, and multiple reflections, which are common in dense, wall-mounted TBE structures or metallic surfaces, can distort the object representation. These disruptive factors represent a fundamental limitation of geometry-based Scan-vs-BIM methods and set natural limits to the reliability of automated results. Additionally, the ambiguity between rotated and displaced components and different components reflects a well-known, fundamental limitation of geometry-based Scan-vs-BIM methods rather than a framework-specific deficiency.

However, another crucial factor influencing the framework's performance is the selection of tolerance values, which need to be predefined in practical applications. In this study, these values were approximated in a practice-oriented manner. While higher tolerances allow components with certain deviations to be classified as identically installed, they may also result in smaller components being incorrectly classified as correctly installed despite significant deviations from the as-planned BIM specifications. Therefore, tolerance parameters need to be adapted in dependence to the quality of the input data, since even identically installed components may show greater deviations in practice than in our dataset. The exact reproducibility of the presented results on other real data sets is therefore not necessarily guaranteed.

One optimization potential was identified in the segmentation process. Initially, only the planned component and the bounding box of the point cloud were compared, which sometimes included noise or neighboring elements. Including all as-planned BIM content within the respective bounding box improved robustness, but further advances in segmentation could significantly reduce misclassifications. A promising option in this context would be automated extraction of component center lines by skeletonization, to improve convex hull analyses.

Another improvement could be achieved by harmonization of the input data. Virtual laser scans of the as-planned BIM, taken from the same positions as the real scans, could minimize occlusion effects and create more comparable datasets. In addition, future work could integrate machine learning techniques, potentially trained on synthetic datasets, to enhance the robustness of component classification and better distinguish between complex displacement and replacement scenarios.

By addressing the identified limitations and exploring advanced optimization strategies, this approach could provide a powerful tool for the validation of TBE systems and contribute to greater efficiency and accuracy in the creation of Dtw. However, we believe that our method already provides an effective advantage for the creation of DTw under the conditions presented.

CC BY

DECLARATION OF COMPETING INTEREST

The authors declare that they have no known competing financial interests or personal relationships that could have appeared to influence the work reported in this paper.

ACKNOWLEDGMENTS

The authors gratefully acknowledge the financial support of the German Federal Ministry for Economic Affairs and Climate Action in the project "EnOB: EnergyTWIN - Energiediagnosestecker Digitaler Zwilling. Neue sensorgestützte und KI-basierte Methoden für die digitale, BIM-basierte Inbetriebnahme von technischen Anlagen in Hochbauwerken und deren energetische Systemoptimierung" (reference number 03EN1026)

DATA AVAILABILITY

Data will be made available on request.

REFERENCES

Abreu, N., Pinto, A., Matos, A. and Pires, M. (2023). Procedural point cloud modelling in Scan-to-BIM and Scan-vs-BIM applications: A review. ISPRS International Journal of Geo-Information, 12(7), 260. https://doi.org/10.3390/ijgi12070260

Anil, E. B., Tang, P., Akinci, B. and Huber, D. (2013). Deviation analysis method for the assessment of the quality of the as-is Building Information Models generated from point cloud data. Automation in Construction, 35, 507–516. https://doi.org/10.1016/j.autcon.2013.06.003

Arayici, Y., Onyenobi, T. and Egbu, C. (2012). Building Information Modelling (BIM) for Facilities Management (FM). International Journal of 3-D Information Modeling, 1(1), 55–73. https://doi.org/10.4018/ij3dim.2012010104

Becker, R., Blut, C., Emunds, C., Frisch, J., Heidermann, D., Kinnen, T., Lenz, A., Möller, M., Pauen, N., Rettig, T., Schlütter, D., Wenthe, M., Blankenbach, J., Bleimann-Gather, G., Fütterer, J., Jungedeitering, J. and van Treeck, C. (2022). BIM-assisted, automated processes for commissioning in building services engineering. In Proceedings of the 39th International Symposium on Automation and Robotics in Construction, Bogotá, Colombia (pp. 558–565). https://doi.org/10.22260/ISARC2022/0079

Besl, P. J., & McKay, N. D. (1992). Method for registration of 3-D shapes. In Sensor fusion IV: control paradigms and data structures (Vol. 1611, pp. 586-606). Spie.

Blut, C., Becker, R., Kinnen, T., Schluetter, D., Emunds, C., Frisch, J., Heidermann, D., Wenthe, M., Rettig, T., Baranski, M., van Treeck, C. and Blankenbach, J. (2024). Optimizing building energy systems through BIM-enabled georeferenced digital twins. The International Archives of the Photogrammetry, Remote Sensing and Spatial Information Sciences, XLVIII-4/W11-2024, 1–8. https://doi.org/10.5194/isprs-archives-xlviii-4-w11-2024-1-2024

Bosché, F., Guillemet, A., Turkan, Y., Haas, C. T. and Haas, R. (2014). Tracking the built status of MEP works: Assessing the value of a Scan-vs-BIM System. Journal of Computing in Civil Engineering, 28(4), Article 05014004. https://doi.org/10.1061/(asce)cp.1943-5487.0000343

buildingSMART Technical. (2024, November 10). IFC GUID - buildingSMART Technical. https://technical.buildingsmart.org/resources/ifcimplementationguidance/ifc-guid/

Chen, J., Jönsson, P., Tamura, M., Gu, Z., Matsushita, B. and Eklundh, L. (2004). A simple method for reconstructing a high-quality NDVI time-series data set based on the Savitzky–Golay filter. Remote Sensing of Environment, 91(3-4), 332–344. https://doi.org/10.1016/j.rse.2004.03.014

Chen, J. and Yong K. C. (2018). Point-to-point comparison method for automated scan-vs-bim deviation detection. In Proceedings of the 2018 17th International Conference on Computing in Civil and Building Engineering, Tampere, Finland (Vol. 2018, pp. 5–7).

Chuang, T.-Y. and Yang, M.-J. (2023). Change component identification of BIM models for facility management based on time-variant BIMs or point clouds. Automation in Construction, 147, 104731. https://doi.org/10.1016/j.autcon.2022.104731

CC BY

Fisher, R. A. (1915). Frequency distribution of the values of the correlation coefficient in samples from an indefinitely large population. Biometrika, 10(4), 507. https://doi.org/10.2307/2331838

German Institute for Standardization (DIN) (2024-05). DIN 18710-1: "Engineering geodesy: Part 1: General requirements" (18710-1).

Gumhold, S., Wang, X. and MacLeod, R. S. (2001). Feature extraction from point clouds. IMR, 2001, pp. 293–305.

Hoffmann, R. and Wolff, M. (2014). Intelligente Signalverarbeitung 1: Signalanalyse (2nd ed.). Springer-Verlag.

Hu, Z., & Brilakis, I. (2024). Matching design-intent planar, curved, and linear structural instances in point clouds. Automation in Construction, 158, 105219. https://doi.org/10.1016/j.autcon.2023.105219

Hu, Z., Pan, Y., Brilakis, I., & Borrmann, A. (2024). Complex Instance Segmentation in Point Clouds with Images and 3D Models. https://doi.org/10.17863/CAM.110935

International Organization for Standardization (ISO) (2023, July 24). ISO 5725-1:2023-07 "Accuracy (trueness and precision) of measurement methods and results. General principles and definitions".

Jia, S., Liu, C., Wu, H., Guo, Z., & Peng, X. (2024). Towards accurate correspondence between BIM and construction using high-dimensional point cloud feature tensor. Automation in Construction, 162, 105407. https://doi.org/10.1016/j.autcon.2024.105407

Jiang, Z., Shen, X., Ibrahimkhil, M. H., Barati, K. and Linke, J. (2022). Scan-vs-BIM for real-time progress monitoring of bridge construction project. ISPRS Annals of the Photogrammetry, Remote Sensing and Spatial Information Sciences, X-4/W3-2022, 97–104. https://doi.org/10.5194/isprs-annals-x-4-w3-2022-97-2022

Kalasapudi, V. S., Turkan, Y. and Tang, P. (2014). Toward automated spatial change analysis of MEP components using 3D point clouds and as-designed BIM models. In 2014 2nd International Conference on 3D Vision (pp. 145–152). IEEE. https://doi.org/10.1109/3dv.2014.105

Kawashima, K., Kanai, S. and Date, H. (2013). Automatic recognition of piping system from laser scanned point clouds using normal-based region growing. ISPRS Annals of the Photogrammetry, Remote Sensing and Spatial Information Sciences, II-5/W2, 121–126. https://doi.org/10.5194/isprsannals-ii-5-w2-121-2013

Kawashima, K., Kanai, S., & Date, H. (2014). As-built modeling of piping system from terrestrial laser-scanned point clouds using normal-based region growing. Journal of Computational Design and Engineering, 1(1), 13–26. https://doi.org/10.7315/JCDE.2014.002

Kellner, M., Vassilev, H., Busch, A., Blaskow, R., Ferrandon Cervantes, M., Poku-Agyemang, K. N., Schmitt, A., Weisbrich, S., Maas, H.-G., Neitzel, F., Reiterer, A. and Blankenbach, J. (2024). Scan2bim - A review on the automated creation of semantic-aware geometric as-is models of bridges. Allgemeine Vermessungs-Nachrichten : AVN. Advance online publication. https://doi.org/10.14627/avn.2024.3.4

Kim, B., Jo, I., Ham, N. and Kim, J. (2024). Simplified Scan-vs-BIM frameworks for automated structural inspection of steel structures. Applied Sciences, 14(23), 11383. https://doi.org/10.3390/app142311383

Kim, S., Kim, S. and Lee, D.-E. (2020). 3d point cloud and BIM-based reconstruction for evaluation of project by as-planned and as-built. Remote Sensing, 12(9), 1457. https://doi.org/10.3390/rs12091457

Kinnen, T., Blut, C., Effkemann, C. and Blankenbach, J. (2023). Thermal reality capturing with the Microsoft HoloLens 2 for energy system analysis. Energy and Buildings, 288, 113020. https://doi.org/10.1016/j.enbuild.2023.113020

Lehmann, R. (2023). Geodätische und statistische Berechnungen. Springer Spektrum. https://doi.org/10.1007/978-3-662-66464-3

Lin, S., Duan, L., Jiang, B., Liu, J., Guo, H. and Zhao, J. (2025). Scan vs. BIM: Automated geometry detection and BIM updating of steel framing through laser scanning. Automation in Construction, 170, 105931. https://doi.org/10.1016/j.autcon.2024.105931

Martens, J. and Blankenbach, J. (2023). Vox2bim+ - A fast and robust approach for automated indoor point cloud segmentation and building model generation. PFG – Journal of Photogrammetry, Remote Sensing and Geoinformation Science, 91(4), 273–294. https://doi.org/10.1007/s41064-023-00243-1

Meyer, T., Brunn, A. and Stilla, U. (2022). Change detection for indoor construction progress monitoring based on BIM, point clouds and uncertainties. Automation in Construction, 141, 104442. https://doi.org/10.1016/j.autcon.2022.104442

Nguyen, C. H. P. and Choi, Y. (2018). Comparison of point cloud data and 3D CAD data for on-site dimensional inspection of industrial plant piping systems. Automation in Construction, 91, 44–52. https://doi.org/10.1016/j.autcon.2018.03.008

Park, S., Ju, S., Yoon, S., Nguyen, M. H. and Heo, J. (2021). An efficient data structure approach for BIM-to-point-cloud change detection using modifiable nested octree. Automation in Construction, 132, 103922. https://doi.org/10.1016/j.autcon.2021.103922

Pătrăucean, V., Armeni, I., Nahangi, M., Yeung, J., Brilakis, I. and Haas, C. (2015). State of research in automatic as-built modelling. Advanced Engineering Informatics, 29(2), 162–171. https://doi.org/10.1016/j.aei.2015.01.001

Riegl. (2017). DataSheet VZ-400. http://www.riegl.com/uploads/tx_pxpriegldownloads/10_DataSheet_VZ-400_2017-06-14.pdf

Rusu, R. B., Blodow, N. and Beetz, M. (2009). Fast point feature histograms (FPFH) for 3D registration. 2009 IEEE International Conference on Robotics and Automation, Kobe, Japan (2009 IEEE International Conference on Robotics and Automation, Kobe, Japan), 3212–3217. https://doi.org/10.1109/robot.2009.5152473 (Original work published 2009)

Savitzky, A. and Golay, M. J. E. (1964). Smoothing and differentiation of data by simplified least squares procedures. Analytical Chemistry, 36(8), 1627–1639. https://doi.org/10.1021/ac60214a047

Schiefer, H. and Schiefer, F. (2018). Statistik für Ingenieure. Springer Fachmedien Wiesbaden. https://doi.org/10.1007/978-3-658-20640-6

Tan, Y., Chen, L., Huang, M., Li, J. and Zhang, G. (2024). Automated geometric quality inspection for modular boxes using BIM and LiDAR. Automation in Construction, 164, 105474. https://doi.org/10.1016/j.autcon.2024.105474

Tao, F. and Qi, Q. (2019). Make more digital twins. Nature, 573(7775), 490–491. https://doi.org/10.1038/d41586-019-02849-1

Tran, H. and Khoshelham, K. (2019). Building. change detection through comparison of a LiDAR scan with a building information model. The International Archives of the Photogrammetry, Remote Sensing and Spatial Information Sciences, XLII-2/W13, 889–893. https://doi.org/10.5194/isprs-archives-xlii-2-w13-889-2019

Wang, B., Lin, F., Li, M., Liang, Z., Chen, Z., Wang, M. Cheng, J. C. (2025). Informative as-built modeling as a foundation for digital twins based on fine-grained object recognition and object-aware Scan-vs-BIM for MEP scenes. Advanced Engineering Informatics, 65, 103382. https://doi.org/10.1016/j.aei.2025.103382

Xie, W., Zhang, Z., Wang, Y., Zhang, Y. and Zhu, L. (2020). The new fast point feature histograms algorithm based on adaptive selection. Journal of Applied Science and Engineering, 23(2), 225–232. https://doi.org/10.6180/jase.202006_23(2).0006

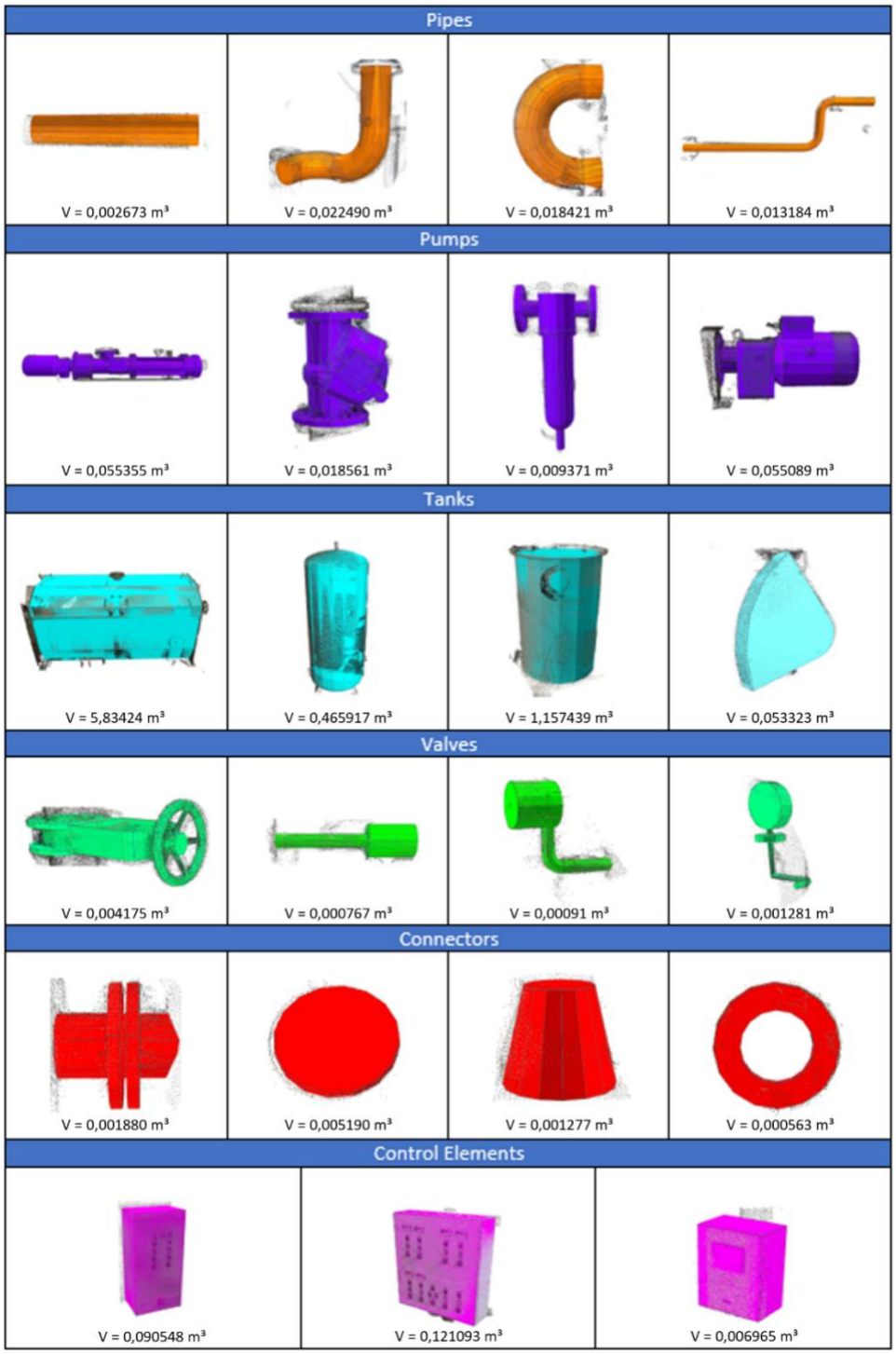
Witte, B., Sparla, P., & Blankenbach, J. (2020). Vermessungskunde für das Bauwesen mit Grundlagen des Building Information Modeling (BIM) und der Statistik (9., neu bearbeitete und erweiterte Auflage). Wichmann. http://www.content-select.com/index.php?id=bib_view&ean=9783879076581

Zhang, Z. (2021). Iterative Closest Point (ICP). In Computer Vision (2nd ed., pp. 718–720). Springer International Publishing. https://doi.org/10.1007/978-3-030-63416-2_179

CC BY

APPENDIX

Table A1: Representation of the object categories of the real-world dataset with IFC model objects and the corresponding segmented point clouds, annotated with object volumes (V).



CC BY

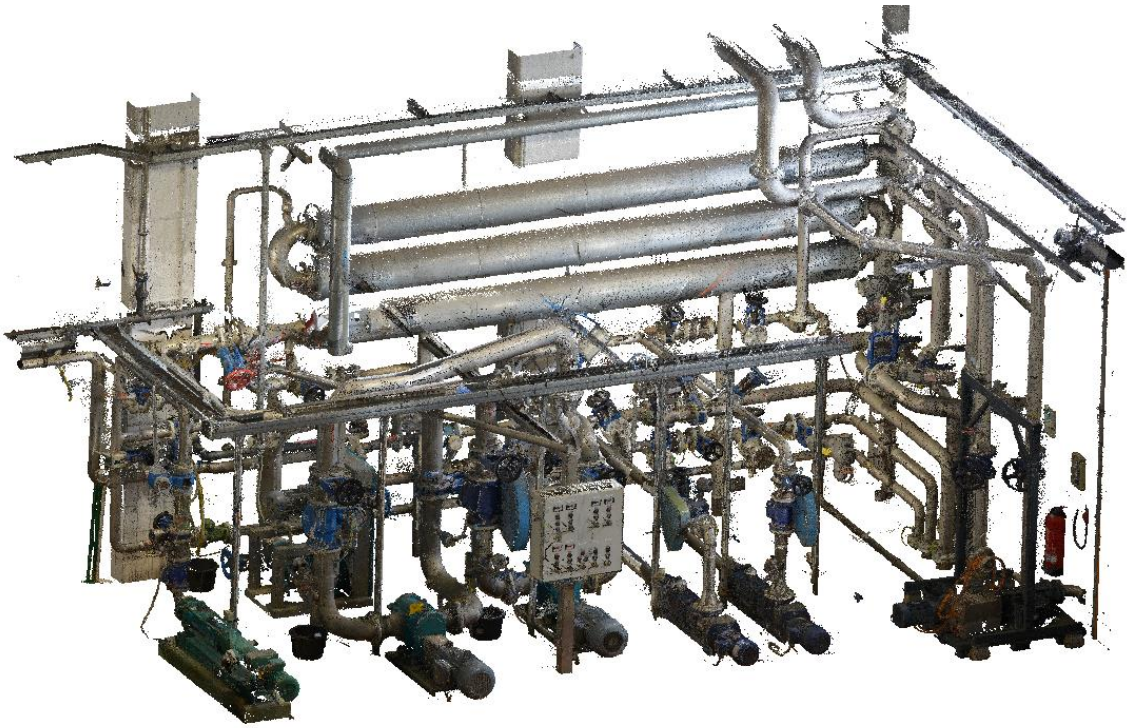


Figure A1: As-built point cloud of the real world dataset.

CC BY